University of Nevada, Reno

Hydrologic and Vegetative Modeling of Vernal Pools in the Sierra Nevada

A thesis submitted in partial fulfillment of the
requirements for the degree of Master of Science in
Hydrogeology

By Ashton Montrone

August, 2013

UNIVERSITY OF NEVADA RENO

THE GRADUATE SCHOOL

We recommend that the thesis
prepared under our supervision by

Ashton Montrone

entitled

Hydrologic and Vegetative Modeling of Vernal Pools in the Sierra Nevada

be accepted in partial fulfillment of the
requirements for the degree of

MASTER OF SCIENCE

Laurel Saito, Ph.D., Advisor

Peter Weisberg, Ph.D., Committee Member

Michael Rosen, Ph.D., Committee Member

Greg Pohll, Ph.D., Graduate School Representative

Marsha H. Read, Ph.D., Dean, Graduate School

August, 2013

Abstract:

Vernal pools are ephemeral wetlands that exist in local geographic depressions with relatively impermeable substrates. Vernal pools are typically filled with water primarily from direct precipitation in the winter and spring months and are dried because of evaporation and seepage in the summer and fall months. The unusual hydrology of vernal pools has led to unique species compositions within the pool as few plant species can tolerate the hydrologic extremes found in vernal pools. Of the roughly 100 different species of plants often found in California vernal pools, 90% are native and 55% are endemic to California. Land use changes and climate change threaten vernal pools. Understanding the impacts of climate change to vernal pool hydrology and the plant community will be important for managing these sensitive ecosystems. Previous vernal pool modeling efforts have been limited to hydrologic quantification while qualitatively discussing the impacts to vegetation. Creating coupled hydrologic and vegetative models is critical to quantitatively understanding impacts to vernal pool vegetation.

A mass balance hydrologic model was created that uses precipitation and temperature as climate inputs and generates a pool stage time-series as an output. Three vegetation models were created from an existing plant community classification system. The vegetation models use the pool stage time-series from the hydrologic model to estimate a vegetative community distribution within the pool. Bias-corrected data from three global climate models (GCM) were used as climate inputs for coupled models of vernal pool hydrology and plant community

distribution. Climate data from the years 1991-2000 and 2091-2100 for the A2 and B1 emission scenarios from each GCM were used. Changes in plant communities were compared between the 1991-2000 and 2091-2100 time segments for each emission scenario.

The hydrologic model results indicate that predicted average annual maximum depth in 2091-2100 did not significantly differ from current conditions under either the A2 or B1 emission scenario. Hydroperiod was predicted to significantly decrease under the A2 scenario, but not under the B1 scenario. Vegetative model results indicate that the pool area containing plant communities associated with vernal pool specialists decreased under the A2 and B1 emission scenarios with the decrease more pronounced under the A2 scenario. Overall, the study indicates that creating coupled hydrologic and vegetation models for vernal pools provide insight on potential impacts of hydrology and climate change on vernal pool plant communities, but modles of sensitive hydrologic systems like vernal pools require climate data with high spatial and temporal resolution.

Acknowledgements:

My graduate education and research would not have been possible without generous funding. The majority of my funding came from the Nevada Agricultural Experimental Station via the Hatch grant. I also received assistance from the College of Agriculture, Biotechnology, and Natural Resources' Jay Dow Sr. Memorial Scholarship.

Our group's research was initiated by Kyle Merriam of the United States Forest Service (USFS). I would like to thank her for orchestrating access to the pools and USFS equipment. Peter Weisberg secured the Hatch grant that provided my funding. I am grateful for his invaluable assistance guiding the research with his vast knowledge of ecology as well as access to equipment, lab personnel, and vehicles. I would especially like to extend my deep gratitude to my advisor, Laurel Saito. Her guidance through reviewing modeling, editing writing, and providing feedback on presentations are hard to overstate. I am grateful for her patience, responsiveness, and moral support. I would like to thank Greg Pohll for his adept modeling insight, reviewing my assumptions, as well as providing software access and support. I would also like to thank Michael Rosen for his ideas for improving experimental design as well as loaning me pressure transducers, even if the weather was uncooperative. I am very appreciative of John Mejia and his student Daniel McEvoy for providing climate data. I would like to thank Bob Blank for his advice and

analysis regarding the soils at the vernal pools. Chris Daly provided daily climate data from his group's PRISM database. This was invaluable for construction and execution of the modeling and I cannot thank him enough.

I would like to recognize Mirte Iubelt for her support of my research as well as access to her own related research. I am grateful for her help installing and maintaining equipment, performing infiltration tests and analysis, as well as her friendship. I would also like to thank Aaron Coogan, Joel Rupp, and Ben Trustman for their assistance installing grazing enclosures, downloading data, and collecting seed cores. Tom Dilts was very helpful providing GIS and GPS support and troubleshooting. I would like to recognize civil engineering technician Brian Hindman of the USFS for working long hours surveying the pools with me. I would also like to thank Meredith Gosejohan for her assistance collecting data and analysis that helped drive the vegetation modeling portion of my project.

I would like to acknowledge Tilly Montrone for helping me through the writing process. Last and certainly not least, I would like to extend appreciation and love to my wife Alexis Montrone. Not only did she volunteer as a field assistant, but her moral support throughout my undergraduate and graduate education has been tremendous.

Table of Contents

List of Tables

List of Figures

Chapter I. Introduction

Defining vernal pools

The research described in the thesis addresses the hydrology and ecology of vernal pools in the Sierra Nevada mountains. Vernal pools are ephemeral wetlands that exist in local geographic depressions with relatively impermeable substrates. In temperate regions experiencing winter snowfall, they are subject to four distinct seasons: they fill with snow in the winter, melt into inundated pools in the spring, become unsaturated and vegetated by summer, then dry and become fully desiccated by fall. Their main source of water is direct precipitation, though some pools receive water from runoff from a very small watershed (Keeley and Zedler, 1998).

The substrates of vernal pools can be bedrock such as volcanic mud or lava flows, clay rich soils, cemented mudflow, and soils with hard clay pans or duripans (Hobson and Dahlgren, 1998; Keeley and Zedler, 1998; Smith and Verrill, 1998; Boone et al., 2006). All of these substrates have low hydraulic conductivities. As these low permeability substrates restrict the infiltration of water, relatively little precipitation can produce perched zones of saturation and pooling of water (Rains et al., 2008).

The morphology of soils in northern California vernal pools is often controlled by ferrolysis, clay formation and translocation, duripan formation, and calcium

carbonate formation (Hobson and Dahlgren, 1998). Ferrolysis occurs when soils alternate between aerobic and anaerobic conditions. When the soils are inundated with water, they become anaerobic which creates a reducing environment. In this environment, free iron is reduced to ferrous iron (Fe^{2+}) and displaces base cations. Base cations, silicates, and bicarbonate move downward in the soil profile and precipitate out of solution as the pool dries. This process forms a duripan (Figure 1) which is thickest in the deepest parts of the pool and tapers towards the margins of the pool basin (Hobson and Dahlgren, 1998). Energy for the ferrolysis cycle is supplied by oxidation of organic material. When the ferrous iron is oxidized, hydroxide and hydrogen ions are created and displace exchangeable ferrous iron which destroys some of the clay minerals. Paradoxically, the increase in hydrogen ions also leads to a lower pH which increases weathering and thus the formation of more clay, primarily kaolinite (Brinkman, 1970; Hobson and Dahlgren, 1998).

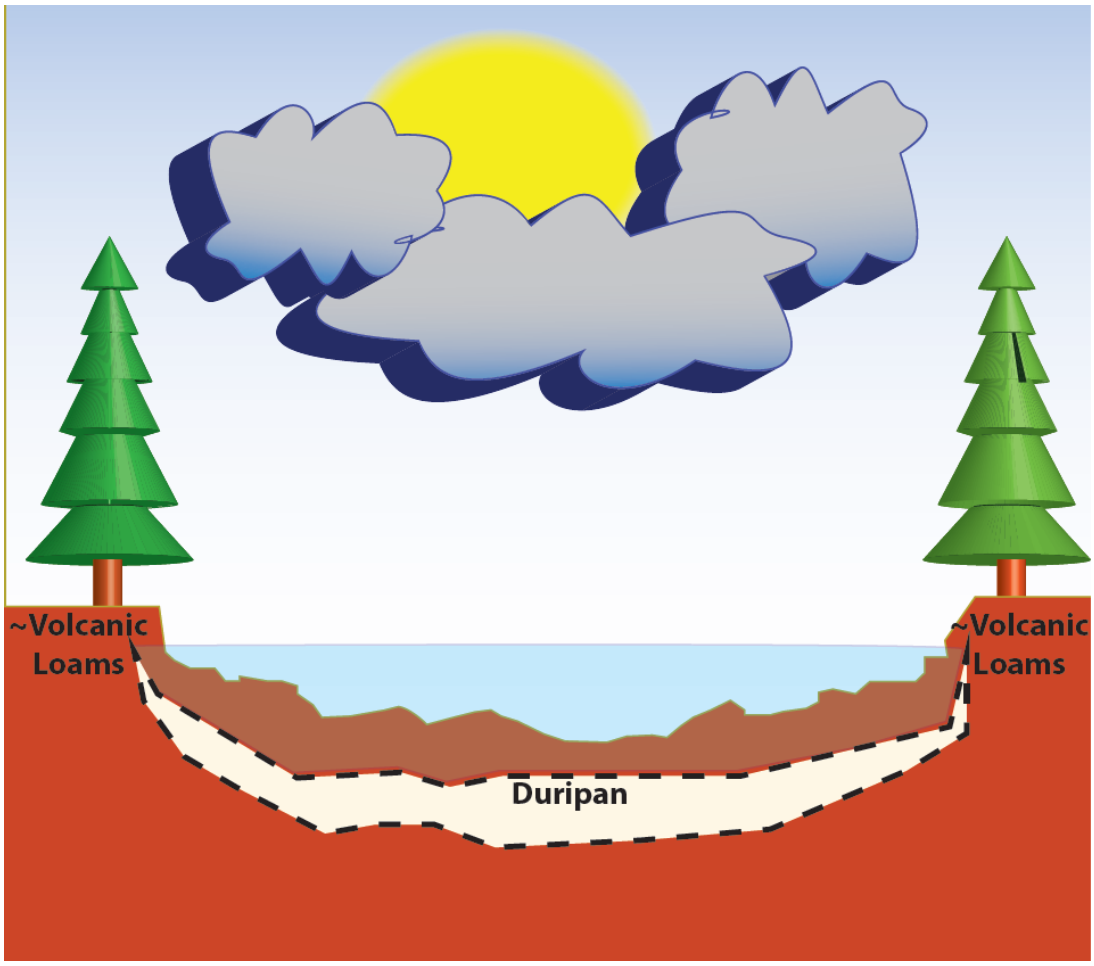

Figure 1. Conceptualization of a volcanic vernal pool in cross-section.

Ferrolysis is the pedogenic process that creates the duripan. Soils are loamy near the soil surface and fine as they move downward in the soil profile towards the duripan. The duripan is orders of magnitude more impermeable than the overlying soil

The clay particles created during weathering move downward in the soil profile when the soil is saturated. As the soil profile matures, a gradient of soil texture where soil is coarser near the surface and finer soil is near the duripan develops (Hobson and Dahlgren, 1998). This texture gradient can make soil infiltration during dry conditions higher than expected through what is commonly referred to

as the “ink bottle effect.” The ink bottle effect results when pores are larger higher in the soil profile than below. The smaller pore radii below have a higher water matric potential than the larger pore radii above. This higher water matric potential below draws the water down more quickly than if the soil profile was homogeneous. This results in relatively fast infiltration rates (Hillel, 1998). As the ink bottle effect is driven by capillary forces, it is a phenomenon that is subject to hysteresis. Pores of this geometry will fill at a smaller matric potential than they will empty. For vernal pools, a larger matric potential required to remove water from the soil would allow plants with the capability to exert large water potentials access to water for a longer period than a soil with a non-tapering pore geometry (Hillel, 1998).

It should be noted that the ferrolysis cycle, clay translocation, and duripan creation are not processes that create vernal pools, but rather a series of positive feedbacks that further develop the soil conditions required for a vernal pool. The origin and time required to create vernal pools is unknown (Holland and Jain, 1988).

The ephemeral nature of vernal pools is also tied to climate. As many lakes have an impermeable substrate, vernal pools are distinguished by the source and seasonality of their water inputs. Vernal pools are often associated with climates that have a majority of their precipitation in the cooler months of the winter and hot dry summers (Keeley and Zedler, 1998). Climates that contain mild wet winters and hot dry summers are sometimes referred to as Mediterranean climates.

While many vernal pools are found in California and the surrounding region, vernal pools are found in other regions with a similar climate such as Chile, South Africa, and Australia (Keeley and Zedler, 1998). Vernal pools are also found to a lesser extent in regions not associated with Mediterranean climates such as Minnesota (Boone et al., 2006), the Lizard Peninsula in south-west Britain (Maclean et al., 2012), Stone Mountain in Georgia (McVaugh, 1943), and New England (Brooks and Hayashi, 2002).

Because vernal pools have seasonally distinct climatic conditions, i.e. alternating between inundation and desiccation for months at a time, unique plant communities are found within the pools. Vernal pool plant species must cope with inundated conditions during the time of seed germination and seedling establishment, and also rapid desiccation in early summer and a short growing season. Many species of wetland plants are not found in vernal pools because of an inability to tolerate the the severe soil desiccation and heat stress that occurs within the pools. Conversely, many upland grasses that can tolerate soil desiccation cannot tolerate inundation (Keeley and Zedler, 1998). The wide range of soil water conditions within vernal pools has helped them remain relatively resistant to exotic species invasion (Spencer and Riesberg, 1998). Of the roughly 100 different species of plants often found in California vernal pools, 90% are native and 55% are endemic to California (Clark et al., 2008). Vernal pools also are floristically diverse and have relatively high indices for species richness (Holland and Jain, 1988).

There are four main life history stages for most vernal pool specialists: seedling, flowering or fruiting, dead or drying with seeds dispersed, and seed dormancy (Bliss and Zedler, 1998; Holland and Jain, 1998). Some vernal pool specialists' seeds require complete submergence to germinate while others do not (Holland and Jain, 1998). A variety of environmental variables provide species specific cues to initiate seed germination including, but not limited to, period of inundation (Bliss and Zedler, 1998), soil moisture (Bauder, 2000), temperature (McLaughlin, 1974), hypoxia (Keeley, 1988), aeration, and light quality (Holland and Jain, 1998). Many of the endemic vernal pool specialists experience limited growth while submerged (Zedler, 1990). The foliage they produce in their aquatic form is often distinct from their terrestrial form (Keeley and Zedler, 1998, Keeley 1990). As the pools dry in the late spring and early summer, the plants continue growing and flower (Holland and Jain, 1988). In Lin's (1970) thesis, many vernal pool specialists died and dispersed seeds between one and two months following pool drying. For pools in the Sierra Nevada, this corresponds to late summer or early fall. After dispersal, the seeds become dormant until germination conditions are satisfactory. Seed dormancy is a mechanism that protects the plant from germinating without satifactory conditions (Bliss and Zedler, 1998) and therefore seeds can remain viable for multiple years.

Annual grassland species are found more often above the high water line, whereas vernal pool specialists are usually found below the high water line (Bauder, 2000). This relationship between vegetation and hydrology results in

vernal pool vegetation often creating concentric rings of differing plant communities. These plant communities transition from one to another along topographic gradients based on hydrologic thresholds. Vernal pool vegetation distribution varies from year to year depending on climatic forcings such as precipitation amount and timing as well as temperature (Brooks, 2004). Thus, hydrology and climate are very important for vernal pool ecosystems.

Annual variations in hydrology and climate are also arguably more critical to vernal pools than lakes. Water found in a lake is usually an amalgamation of sources that vary widely in spatial and temporal origin, many of which carry over from year to year. These sources often include groundwater, stream inflows, and direct precipitation. Precipitation is the source of water for groundwater and streamflow. Groundwater and streamflow can integrate precipitation over many years with complex interactions, i.e. streamflow contributing to groundwater and groundwater discharging to streamflow (Dingman, 2002). Because of the potentially long transport time associated with travelling underground, precipitation can travel for multiple years before arriving in a lake. This integration of precipitation across multiple years dampens the effect of annual variability of precipitation on the water budget to a lake. This damping can provide a buffer for lakes from extremely wet or dry years. Furthermore, for large lakes, lake storage provides an additional buffer to climatic variability. As vernal pools' primary source of water is direct precipitation and they do not carry storage from one year to the next, they do not have year to year storage or long travel times to buffer their water budget. The

result is a system that exhibits strong interannual variability and is extremely sensitive to climatic change (Brooks, 2004). Sensitive systems such as vernal pools can therefore theoretically respond more quickly to climatic changes than other more common buffered systems via changes in hydrology and the resulting plant community.

There are several threats to the Sierra Nevada vernal pools, including climate change, land-use change, and human-induced activities such as grazing. Dettinger and Cayan (1995) showed that the temperatures in the Sierra Nevada increased between 1940 and 1995, and Cayan et al. (2001) showed temperatures increased for the same region between 1947 and 1994. Dettinger and Cayan (1995) and Cayan et al. (2001) showed that the winter and spring months increased by roughly 2 ^{0}C while the overall annual temperature difference was near 1.5 ^{0}C for period the study covered. Projections for the 21st century show temperatures increasing by 3 or 4 ^{0}C for the region under a "business as usual" scenario (Stewart et al., 2004). Precipitation did not increase in this area between 1940 and 1995 (Dettinger and Cayan, 1995) and is not projected to change in the Sierra Nevada through the 21st century (Stewart et al., 2004). If these temperature and precipitation projections are correct, the water budget for the vernal pools will likely be affected. If all other variables are held constant, a temperature increase without an increase in precipitation would lead to the pools being filled for a shorter amount of time because the increase in temperature would increase evaporation and have more

precipitation fall as rain instead of snow, leading to earlier snowmelt and desiccation. Without any extra water, the pools will dry up faster.

Ranchers use the forest and the vernal pools to feed and water their cattle. Preliminary research by Marty (2005) suggested that vernal pool specialists such as *Orcuttia tenuis* are more abundant in grazed pools than ungrazed pools. There is a possibility that the cattle are compacting the soil and are effectively decreasing the soil's hydraulic conductivity which is leading to more favorable periods of inundation for vernal pool specialists. If this is the case, that decrease in hydraulic conductivity could slow the rate of water leaving the pools through percolation. Therefore, it has been hypothesized by Pyke and Marty (2005) that cattle grazing could mitigate the effects of climate change on vernal pools.

Previous Vernal Pool Modeling Efforts

Mathematical models provide an approach for adaptive management and conservation of vernal pools in light of the various resource demands and environmental stressors that threaten them. By modeling the pools' hydrology, we can understand what environmental parameters drive the hydrologic system as well as forecast how land-use decisions may affect the pools. Unfortunately, vernal pool hydrology has only rarely been modeled. Previous models include models of pools in Oroville, CA and the Del Sol Preserve near Santa Barbara, CA by Pyke (2004), models of pools in Cloquet, Minnesota by Boone et al. (2006), and models of pools in southwest Britain by Maclean et al. (2012).

For the pools Pyke (2004) modeled, precipitation arrives in the form of rain and the pools are on the order of 500 to 5,000 m^2 in area. His model, PHYDO, uses a mass balance approach with a single pool as the functional unit. Pyke's (2004) governing equation is:

$$\text{Eq 1)} \quad V_t = V_{t-1} + D + R + \Delta S - ET - O \quad [L^3]$$

where V_t is the surface water volume for the current time step and V_{t-1} is the volume of the previous time step. D and R represent direct precipitation onto the water body and precipitation onto the basin in unwetted areas, respectively. ΔS is the change in shallow surface soil water storage, ET is the open water evapotranspiration, and O is the daily overflow. All terms in the equation have units of volume. The geometry used to represent the pools is two orthogonal cross sections intersecting, with each cross section represented by a trapezoid on top of a low angle basal triangle (Figure 2). Each cross section has five points. Figure 2 shows one cross section, with the second being perpendicular to the one shown with point "3" coincident with each cross-section. The model assumes that precipitation onto the vernal pool basin is the only input. Evapotranspiration, groundwater seepage, and pool spillage when full are the outputs.

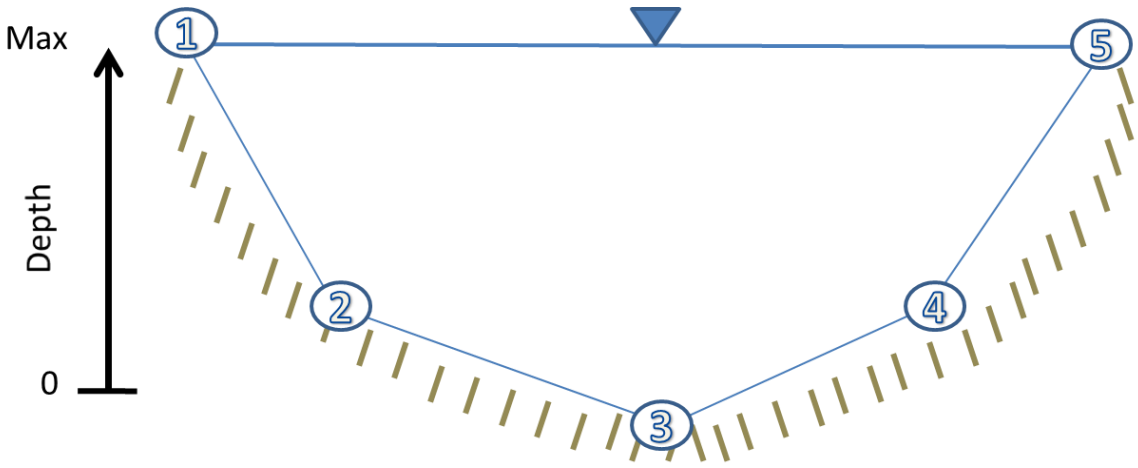

Figure 2. Cross section of Pyke's geometric representation

(Adapted from Pyke, 2004). Numbers represent points of the cross section. Figure is not to scale.

Pyke (2004) broke the ET budget into three portions: evaporation from open water, evaporation from bare soil, and vegetation transpiration. Evaporation from open water is the water that is standing above the ground. Evaporation from bare soil is the evaporation coming from the soil after it has become inundated but no longer has standing water on it. Vegetation transpiration is the water that leaves by transpiration from plants.

Boone et al. (2006) modeled eight pools in Minnesota ranging in size between 500 and 5,000 m^2. These pools receive precipitation in the form of both snow and rain. Boone et al. (2006) also used a mass balance approach with a single pool as the model functional unit. The pool's geometry was approximated by a cylinder. Boone et al.'s (2006) governing equation is rearranged as:

Eq 2) $$S + e = P + SWI - ET - SWO - GWO\ [L^3]$$

where S is storage, e is an error term, P is precipitation, SWI is surface water input, ET is evapotranspiration, SWO is surface water output (from the pool spilling over when above maximum depth), and GWO is groundwater output or seepage with all terms given as volumes. Equation 2 differs from the Pyke (2004) governing equation (Eq. 1) in that it contains an error term as well as a SWI term.

While accepted definitions of vernal pools (e.g. Keeley and Zedler, 1998) indicate an absence of remotely sourced water inputs, mountainous vernal pools systems by virtue of topographic variation receive some amount of water input from adjacent surface runoff. The SWI term is estimated in the Boone et al. (2006) model using the curve number approach from the USDA Soil Conservation Service manual (USDA, 1986). This method estimates runoff with a stepwise function. Boone et al. (2006) used the Priestly-Taylor method as modified by Campbell (1977) to estimate evapotranspiration.

The Maclean et al. (2012) model of vernal pools in Britain is broadly based on Pyke's (2004) model and simulates the hydrology at a daily time-step of a 16 km^2 portion of the Lizard Peninsula in Cornwall, England that contains several vernal pools. This differs from Pyke (2004) and Boone et al.'s (2006) use of a single pool as the functional unit. Pool geometry was delineated from a 1m x 1m LiDAR grid. The relationship between surface area and volume of individual pools was determined

by comparing the LiDAR data set to five functional relationships using the statistical software R. The relationship between area and volume for smaller pools followed the form:

$$\text{Eq 3)} \qquad \text{Area} = \text{a} * \text{volume} \quad [\text{L}^2]$$

where a is a fitting parameter that is iteratively solved for. This approach for smaller pools is similar to Boone et al.'s (2006) approach to pool geometry. For larger pools, the relationships between area and volume followed the form:

$$\text{Eq 4)} \quad \text{Area} = \left(\frac{\text{a}}{1 + \exp(-\text{volume}^{\text{b}})}\right) \quad [\text{L}^2]$$

$$\text{Eq 5)} \quad \text{Area} = \left(\frac{\text{a}}{1 + \exp(-\text{b} * \text{volume})}\right) \quad [\text{L}^2]$$

$$\text{Eq 6)} \quad \text{Area} = \left(\frac{\text{a}}{1 + \exp(-\text{b} * \text{volume}^{\text{c}})}\right) \quad [\text{L}^2]$$

where *b* and *c* are fitting parameters. The selection of the possible functions and values for the parameters *a* and *b* were solved by maximizing r^2 values relative to the LiDAR data. The majority of the pools Maclean et al. (2012) modeled range in size from 10 to 50 m^2.

The Maclean et al. (2012) model assumes four soil layers with assigned thicknesses in addition to the surface water. The four soil layers exchange water

with each other as well as the surface water. For each pool, the volume of surface water is:

$$\text{Eq 7)} \quad V_{0t} = V_{0t-1} + R + I_0 - I_{CRK} - E_0 + Q_1 + \Delta O \quad [L^3]$$

where V_{0t} is the surface water volume at time t, V_{0t-1} is the surface water volume of the preceding day, R is the water received as either direct interception at the flooded surface or as run-off from unflooded areas, I_0 is infiltration to the surface soil layer, I_{CRK} is infiltration through cracks, E_0 is evaporation from surface water, Q_1 is surplus water from the surface soil layer that reaches the surface when the soil layer exceeds field capacity and ΔO is the net volume of water received from or lost to adjacent basins. All terms have the units of volume. Reference surface evaporation was calculated using the Penman-Monteith equation (Allen et al., 1998). Evaporation for each time-step from surface water was defined as a function of depth and given by:

$$\text{Eq 8)} \qquad E_0 = A_0 \left(\frac{a_0}{D_0 + b_0} \right) * ET_0 \quad [L^3]$$

where A_0 is the area of surface water within the basin, D_0 is the mean depth of surface water, a_0 and b_0 are constants, and ET_0 is reference ET. Evaporation from the surface soil layer is given by the equation:

$$\text{Eq 9)} \qquad E_s = A_{bare}\left(\frac{S1_{t-1} - S_{wilt}}{S_{field} - S_{wilt}}\right)^{\delta} * ET_0 \quad [L^3]$$

where A_{bare} is the area of bare soil, $S1_{t-1}$ is the antecedent soil moisture fraction of the surface layer, S_{wilt} is the fractional soil water volume at wilting point, and S_{field} is the fractional soil water volume at field capacity. δ is a constant that is assumed to be four from the findings of Pyke (2004). In Maclean et al.'s (2012) model, each of the four soil layers has a unique water mass balance equation that allows the soil layers to exchange water with each other as well as the surface water.

Precipitation in the Maclean et al. (2012) model was assumed to be uniform across the study area. Similar to Boone et al. (2006), the Natural Resources Conservation Service curve number method was used to determine water contributions from adjacent area to the vernal pools.

While all three models have components that are applicable to Sierra Nevada pools, none are ideally suited to model them. All three models considered pools that were less than 5,000 m^2 in area. Many of the Sierra Nevada pools are an order of magnitude larger (≈50,000 m^2) and have complex topographies that are not adequately represented by simple geometries. Pyke (2004) suggested that some of the differences between modeled predictions and observed values were due to an over-simplified geometry that invalidated the stage to volume relationship. Another factor that limits the previous models' applicability to the Sierra Nevada is that form

of precipitation is not considered. The form of precipitation that arrives at the Sierra Nevada vernal pools is primarily snow.

Although vernal pools and their unique vegetation have been recognized for decades (Jepson, 1925; Keeley and Zedler, 1998) and there have been several studies of their vegetation, the few attempts to model their hydrology may be because of the relatively small amount of water that they contain as well as their fragmented and ephemeral nature. Furthermore, it is probable that the recognition that a vernal pool's vegetation is concomitant with hydrology is the reason that any hydrologic models of vernal pools exist at all. Though all three hydrologic models previously summarized discussed the ecological implications of hydrologic models of vernal pools, none explicitly modeled vegetation. Creating a vegetative model driven by a hydrologic model could give quantitative insight to questions of vernal pool vegetative community, particularly regarding the impacts of climate change.

Research Goals

Because of the presence of endemic vegetation and distinct annual hydrologic patterns of vernal pools, the goals of this research are to determine if a changing climate has the potential to shorten the hydroperiod and impact the vegetation patterns of the vernal pools. With an increase in air temperature, the form of precipitation could change from snow to rain. Even if there is not a change in the form of precipitation, the ET rate could increase for the inundation period which could result in a shorter hydroperiod. If the form of precipitation does change from

snow to rain, the beginning and end of the inundation period could be earlier. If this is the case, while the mean annual air temperature may be higher, the mean air temperature for the time that the pools are inundated may be lower.

Hypothesis 1: If the form of precipitation changes to rain more often than snow, the air temperatures will be lower during the period of inundation.

Hypothesis 2: If the form of precipitation changes to rain more often than snow, the hydroperiod will remain the same or possibly become longer.

Vernal pool specialists such as *O. tenuis* were found in both long term inundated and deep tolerant community types defined by Gosejohan (2012). If there is a change in hydroperiod, it could affect the vernal pool specialists' distribution in the pool.

Hypothesis 3: As hydroperiod decreases, vernal pool specialists will proportionally be found in deeper portions of the pools.

Hypothesis 4: As hydroperiod decreases, vernal pool specialists will have a change in the location of habitat area within the pool.

Hypothesis 5: As hydroperiod decreases, vernal pool specialists will have a change in the total area of habitat.

Site Description

The study area involves two vernal pools in the Sierra Nevada (Figure 3), Coyote Springs and Adobe North in Lassen National Forest where Gosejohan (2012) completed extensive vegetative surveys and monitored water level for a wet season on a stage gauge in spring and summer of 2010. Coyote Springs is roughly 46,000 m^2 and is centered at N 40° 42' 55" E -121° 22' 2" (Figure 4). Adobe North is roughly 56,000 m^2 and is centered at N 41° 13' 42" E-121° 28' 53" (Figure 5). The soils in the region are of volcanic origin (Norris and Webb, 1976). Vernal pools found in volcanic regions are often due to shallow R horizons (Holland and Jain, 1998). According to Web Soil Survey (2012), the soil of Adobe North is a Lasvar-Pitvar complex with clay that extends from the surface to 50 cm and a duripan from 50 cm to 100 cm. Soils for Coyote Springs were identified as the Skalan-Bobbitt families association, which is a cobbly sandy loam to 35 cm, very cobbly loam from 35 cm to 150 cm, and weathered bedrock below that. The soil is defined as well-drained with a moderately high hydraulic conductivity. Both pools are surrounded by coniferous forest comprised of Ponderosa and Jeffrey pine.

Figure 3. Approximate region of the vernal pools within the Western United States.

While Websoil Survey (2012) does not indicate the soils are hydric, the soils are hydric in the general sense. While difficult to formally delineate in vernal pools, broadly speaking hydric soils are soils that are saturated near the surface sufficiently to become anaerobic during the growing season (NRCS, 2013). Hydric soils in vernal pools are delineated using indicators related to a depletion of the soil matrix near the surface within a closed depression and various situational redox

and chroma criteria (Hurt and Vasilas, 2006). Delineating hydric soils in vernal pools is difficult because of high variability in soil characteristics over short distances and masking of redox indicators by iron and the low chroma of young volcanic parent material. It can also be difficult to determine if the redox indicators are modern or from the wetter Pleistocene (Green et al., 2008). Green et al. (2008) maintained that many of the soils in northern California vernal pools are hydric soils.

Figure 4. Aerial view of Coyote Springs (Image source: Google Earth©)

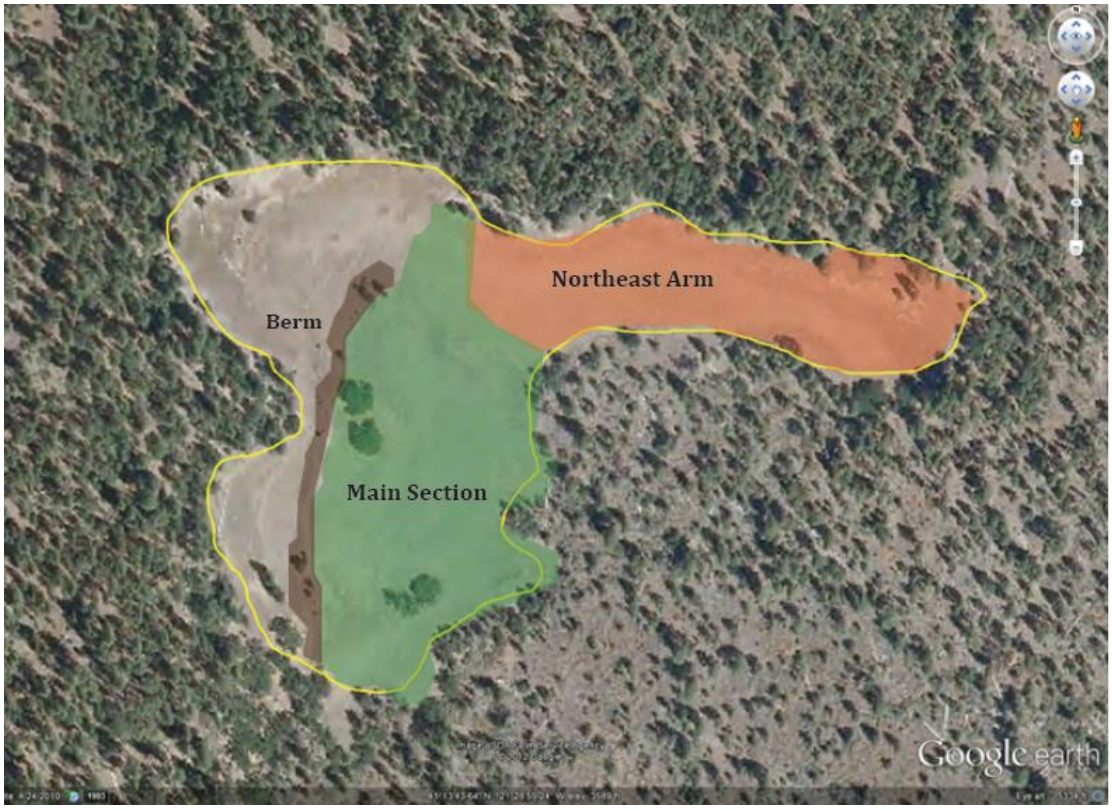

Figure 5. Aerial view of Adobe North (Image source: Google Earth©)

The northeast arm and the main section are separated by a ridge. The main section does not extend to the western edge of the basin because a man-made berm impedes connectivity.

Previous Work

At Coyote Springs and Adobe North, Gosejohan (2012) maintained an onsite camera that took pictures of a stage gage at each pool at four hour resolution for an entire wet season. She also performed a spatial vegetation survey that determined species, density, and other plant health indicators. Gosejohan (2012) coupled the

stage information with the vegetative survey to determine thresholds of hydroperiod tolerance for different vegetative species including the endangered grass, *O. tenuis*.

Gosejohan (2012) performed non-metric multidimensional scaling (NMS) ordination analysis. To minimize noise in the dataset, Gosejohan (2012) removed plant species that occurred in less than 5% of the plots. This removal left 40 plant species for ordination. Her ordination solution was 2-dimensional with axis 1 explaining ≈47% of the variance and axis 2 explaining ≈12% of the variance for a total of ≈58% explained. Axis 1 was strongly correlated with inundation length (r=0.76) and to a slightly lesser extent maximum depth (r=0.67). Axis 2 was slightly correlated with maximum depth (r=0.3).

Gosejohan (2012) performed hierarchical agglomerative cluster and indicator species analyses (Dufrêne and Legendre, 1997). Gosejohan (2012) categorized the 40 plant species occurring in greater than 5% of plots found within both pools into five plant community types: short-term inundated, edge, shallow tolerant, deep tolerant, and long term inundated. These five plant community types were defined by inundation length and maximum depth (Figure 6).

The indicator species for the short-term inundated community are the exotic annual grass *Bromus hordeaceous,* the annual native herb *Helianthus bolanderi,* and the invasive non-native *Lactuca serriola.* The indicator species for the edge community includes the invasive herb *Epilobium brachycarpum,* the native annual

herb *Lotus purshianus,* and the native perennial herb *Poa secunda.* The indicator species for the shallow-tolerant community are the native endemic annual herb *Deschampsia danthonioides* and the native perennial herb *Grindelia nana.* The indicator species for the long-term inundated community include *Castilleja campestris ssp. campestris, Eleocharis bella, Marsilea oligospora, Piluaria americana,Plagiobothyrus stipitatus,* and *Psilocarphus brevissimus.* These are primarily vernal pool specialists and wetland generalists. The indicator species for the deep tolerant community are the native hemiparasitic vine *Cuscuta howelliana* and the native annual herb *Epilobium densiflorum* (Gosejohan, 2012). In general, vernal pool specialists such as *O. tenuis* are characteristic of both the long-term inundated community and the deep-tolerant community.

Gosejohan (2012) performed classification tree analysis (CART) to determine hydrologic thresholds for each plant community group from vegetation survey data from all plots (N=344) from both pools (Figure 6).

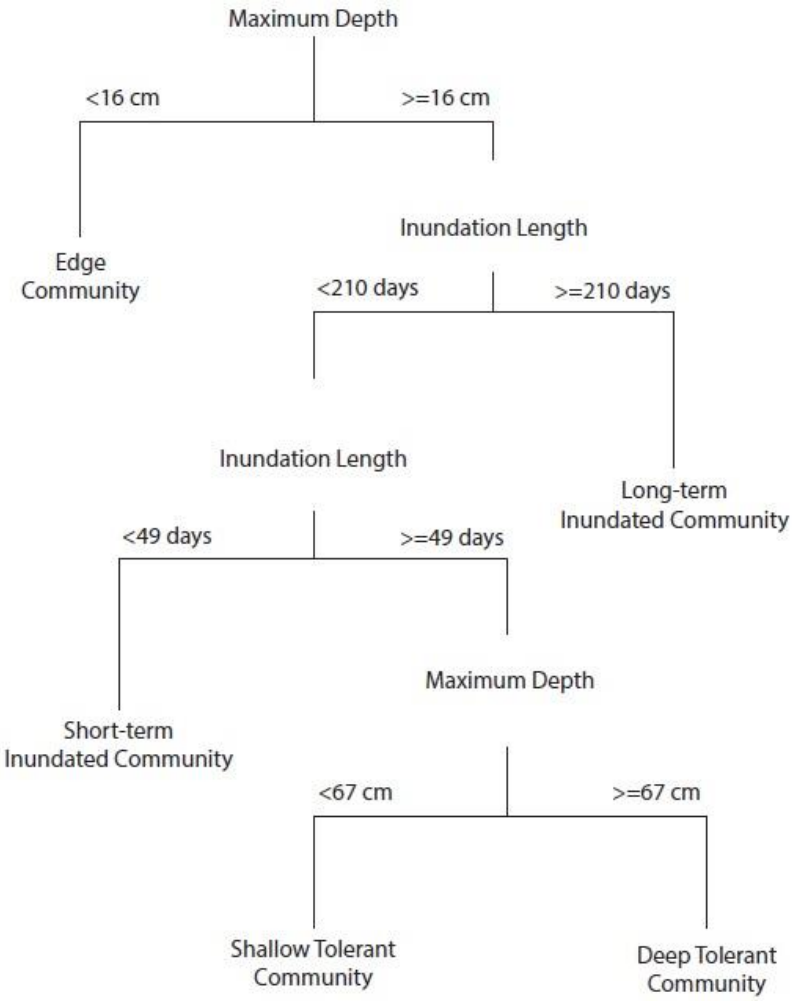

Figure 6. Gosejohan plant model adapted from Gosejohan (2012)

Plant community decision tree based on maximum depth and inundation length

Chapter II: Methods

This chapter describes the field work and data collection that were used to inform model development, including calibaration, simulation of future climate scenarios, and analysis of results. The chapter also contains details of the numerical framework and composition of the hydrologic and vegetative models.

Stage Gauges

Moultrie Game Spy I-65 digital cameras and stage gauges were installed in December 2010 by Meredith Gosejohan at Adobe North and Coyote Springs. The cameras were programmed to take photographs of the stage gauges every four hours. The stage gauges were made from PVC pipe and were attached to steel rebar that was hammered into the ground. The PVC had tape markings at 2 centimeter intervals. Gosejohan (2012) recorded the stage measurement from the photographs from December 4, 2010 to June 27, 2011. To get daily values, one stage measurement was recorded per day from the clearest photograph of the six taken each day (Gosejohan, 2012).

In April 2012, the stage gauges were re-installed and the batteries in the game cameras were replaced. Upon replacing the batteries, the camera reset to default settings which changed the time resolution from taking a picture every four

hours to taking a picture when the motion-detection sensor was triggered. This change in settings resulted in few pictures being taken and many pictures of the stage gauges being obstructed by objects, especially bears. As fewer than 10 data points for stage at each pool were recorded for the water year (WY) 2012, only stage gauge data from WY 2011 were used for calibration.

Total Station Survey and Surface Interpolation

Topographic surveys of both pools were performed in the summer of 2011. A Leica-Wild TC101 total station and Total Data Systems Recon with Survey Pro for Windows XP (Version 3.8.1) data collector were used which has one second accuracy. The vegetation survey was performed on a 25-meter grid and two 10-meter transects. The topographic survey included these vegetation survey points, stage gauges, and significant topographic features such as steep elevation gradients, berms, high points, and the pool perimeters (Figures 7 & 8). The survey data were prepared in the Universal Transverse Mercator (UTM) zone 10 N projection.

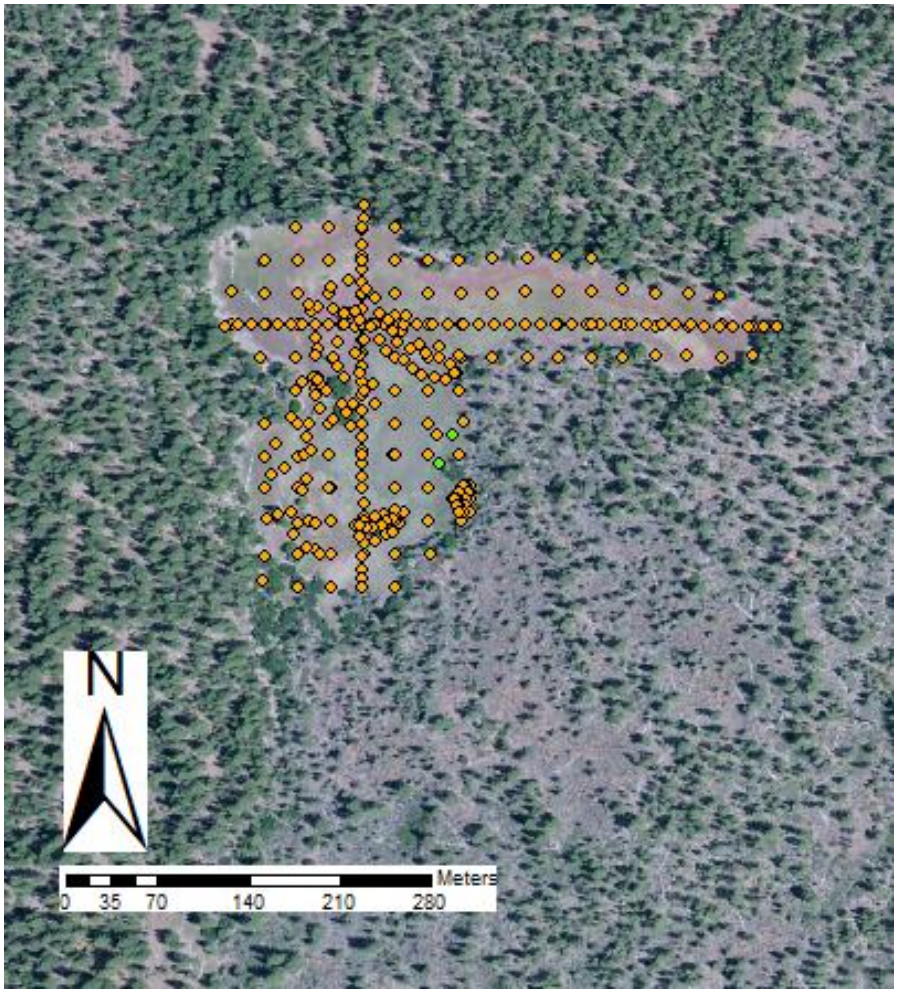

Figure 7. Map of Adobe North

The orange dots are surveyed points and the green dots are the locations of the stage gauges.

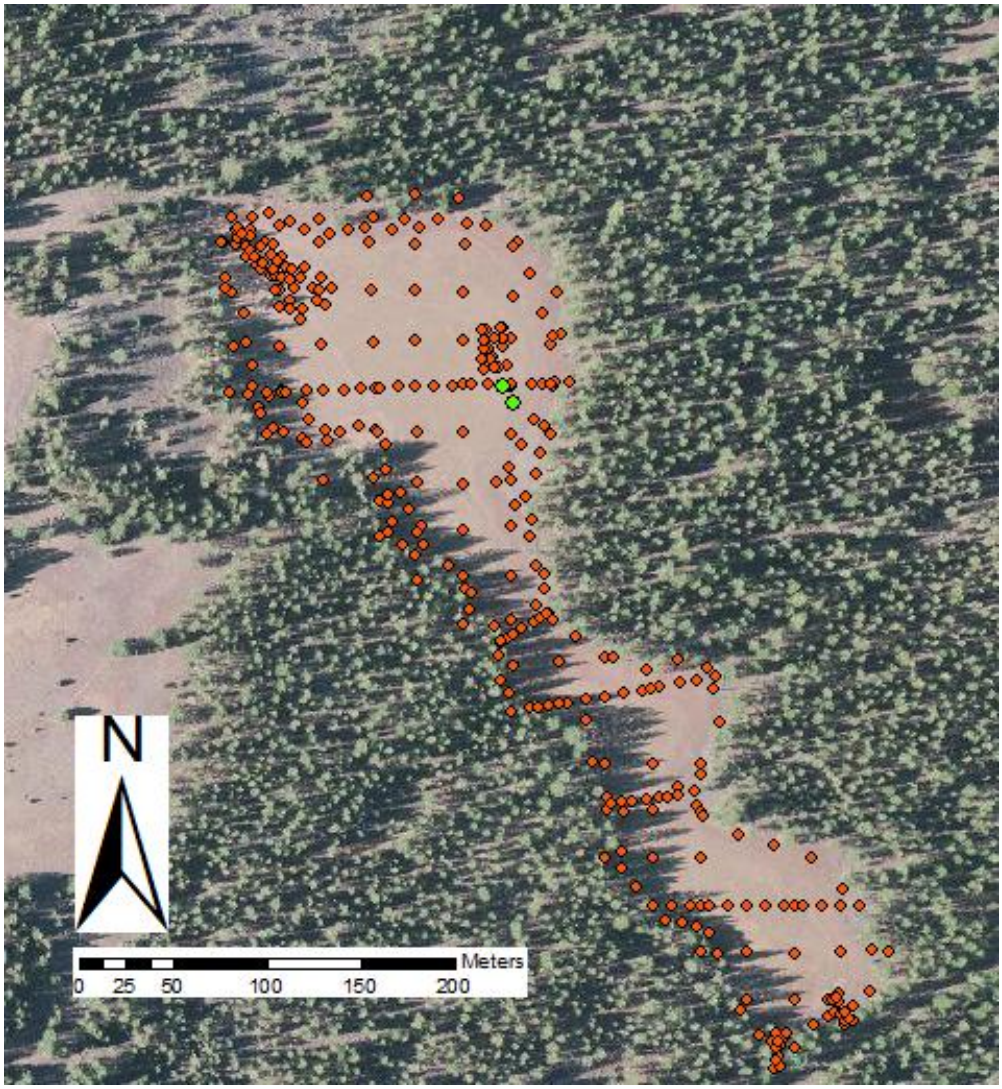

Figure 8. Map of Coyote Springs

The red dots are surveyed points and the green dots are the locations of the stage gauges.

The total station survey data were used to create a surface interpolation and stage:area:volume (S:A:V) relationship using Surfer Version 8.0 for each pool (Golden Software, 2002). The gridding method used was kriging with 2.5 meter grid

resolution for Coyote Springs and a 5 meter grid resolution for Adobe North. A coarser resolution was used for Adobe North because the finer resolution was too short of a grid length to recognize other points on top of the berm. This resulted in the berm being represented as a series of peaks instead of a continuous feature. Using the larger grid length resulted in an interpolation that made the berm a continuous feature. The area and volume from the gridded data were paired with the associated stage and compiled into Tables 1 and 2 for Coyote Springs and Adobe North, respectively.

Volume (m^3)	Area (m^2)	Stage (m)
0	0	0
200	5052	0.02
344	9264	0.04
550	11291	0.06
794	13165	0.08
1077	15169	0.1
1401	17186	0.12
1769	19591	0.14
2187	22131	0.16
2655	24666	0.18
3172	26958	0.2
3732	29109	0.22
4335	31152	0.24
4978	33129	0.26
5661	35251	0.28
6388	37386	0.3
7157	39609	0.32
7974	42112	0.34
8844	44859	0.36
9768	47585	0.38
10749	50634	0.4
11795	53974	0.42
12911	57674	0.44

Table 1. S:A:V relationship of Coyote Springs. Kriging grid resolution for the surface interpolation was 2.5 meters. Volume, area, and stage were calculated for each 2 cm elevation increase from the lowest elevation on the stage gauge. The pool basin area was estimated in ArcGIS and was assumed to be 44,000 m^2 which corresponds to a stage of about 0.36 m.

Volume (m^3)	Area (m^2)	Stage (m)
0	0	0
424	8522	0.02
614	10604	0.04
848	12762	0.06
1124	14850	0.08
1447	17674	0.1
1834	21065	0.12
2285	23931	0.14
2789	26424	0.16
3341	28745	0.18
3941	31289	0.2
4593	33969	0.22
5300	36735	0.24
6064	39604	0.26
6884	42355	0.28
7759	45132	0.3
8689	47873	0.32
9674	50641	0.34
10714	53353	0.36
11806	55882	0.38
12949	58428	0.4
14145	61309	0.42
15404	64708	0.44
16736	68471	0.46
18143	72198	0.48
19624	76067	0.5
21186	79739	0.52
22812	82890	0.54
24497	85536	0.56
26234	88164	0.58
28023	90813	0.6
29870	94027	0.62
31785	97337	0.64
33762	100368	0.66
35799	103399	0.68
379000	106899	0.7

Table 2. S:A:V relationship of Adobe North. Kriging grid resolution for the surface interpolation was 5 meters. Volume, area, and stage were calculated for each 2 cm elevation increase from the lowest elevation on the stage gauge. The pool basin area was estimated in ArcGIS and was assumed to be 56,000 m^2 which corresponds to a stage of about 0.38 m.

Infiltration Tests and Soil Texture

Infiltration tests were performed at six locations in Adobe North and four locations in Coyote Springs in July 2012. More infiltration tests were taken at Adobe North because it is both larger and more heterogeneous than Coyote Springs. Furthermore, during a visit in Spring 2012, Adobe North (Figure 5) was found to be dry in the northeast arm of the pool but was still wet in the south-east main section (Figure 9). To determine if the difference in pool stage between the main section and northeast arm was related to a difference in soil infiltration and texture, four soil tests were performed in the main section of the pool and two tests were performed in the northeast arm. In Coyote Springs, infiltration tests were performed at two sites in the larger northern portion, one site in the middle section, and one site in the southern section (Figure 4).

Infiltration tests were performed the tests using large disk permeameters with a 20.8 cm diameter footprint and one-liter capacity. One-centimeter of tension was applied to the permeameter to prevent flow in macro-pores. A thin (< 1 cm) layer of coarse silica sand mixture was used for leveling the soil surface. Because of fast infiltration rates, water levels within the disk permeameter were recorded every five seconds. Hydraulic conductivities were estimated using the Phillip's equation (Eq. 10; Dingman, 2002).

$$\text{Eq 10)} \quad f(t) = \frac{S_P}{2} * t^{-1/2} + K_P \quad \left[\frac{\text{cm}}{\text{second}}\right]$$

K_p= Phillip's estimation of hydraulic conductivity [cm/sec]
f(t)=infiltration rate [cm/sec]
S_p=Sorptivity [cm/sec]
t=time [sec]

Surface soil samples (approximately the top 5 centimeters) were taken near each infiltration test and were analyzed for soil texture. Prior to particle size analysis, samples were sieved to remove the fraction greater than two millimeters in diameter. Approximately 10 grams of each sample were pre-treated with 30% H_2O_2 to remove organic matter and were then dispersed with $(NaPO_3)_6$. The pre-treated samples were then centrifuged to separate the sands and silts from the clays. The clay fraction was weighed, and sands and silts were then separated by wet sieving. After the sand and silt fraction were separated, they were then dried and weighed. More detail on this soil classification method can be found in Jackson (2005).

Figure 9. Adobe North looking to the northeast arm

The pool was wet in the main body of the pool but dry in the northeast arm on April 21, 2012. The foreground is higher in elevation than the background.

Weather and Climate Data

A weather station was installed on May 5, 2012 and uninstalled on June 5, 2013 at the Coyote Springs vernal pool. The weather station was an assembly developed by Decagon Devices Inc that included a Decagon EM-50 datalogger, Davis anemometer (5% wind speed and 7^0 wind direction accuracy) , PYR total solar radiation sensor (5% accuracy), ECRN-100 high-resolution rain gauge (0.2 mm resolution), and VP-3 humidity(0.1% resolution), temperature(0.1^{0}C resolution),

and vapor pressure sensor (0-47kPa range). The datalogger was set to record measurements from the sensors at one hour intervals. Data were downloaded from the weather station using the ECH$_2$O Utility software provided by Decagon Devices, Inc. Batteries for the EM-50 datalogger were replaced as necessary. As the weather station was installed after WY 2011, it was used to evaluate which climate dataset to use to calibrate the model.

PRISM precipitation and temperature data were used as the climate inputs for the hydrologic model for calibration and historical runs. PRISM provides precipitation and temperature data interpolated to a spatial grid and is distributed by the PRISM climate group at Oregon State University. The spatial resolution is 4 kilometers and data are publically available at a monthly time step (Daly et al., 1994). . Chris Daly of the PRISM Climate Group provided daily climate data covering the period from January 1, 1980 to June 18, 2013.

Daymet precipitation and temperature data was provided by the Desert Research Institute (DRI). The Daymet database is a distribution of precipitation, temperature, water vapor pressure, shortwave radiation, and snow water equivalent data interpolated to a spatial grid that is operated by NASA (Thornton et al., 1997). The data are available at a daily time-step with one kilometer spatial resolution covering the period from January 1, 1980 to December 31, 2011.

Both the PRISM and Daymet datasets were used as climate inputs for calibration of the hydrologic model for WY 2011 by comparing model output to stage gauge

data. Daymet and PRISM climate data were compared to each other as well as calibration parameter results the climate dataset produced. Only PRISM's period-of-record coincided with the weather station's period-of-record, therefore only the PRISM dataset was compared to the weather station's dataset for evaluation purposes. For WY 2011, Daymet predicted nearly double the precipitation that PRISM did for the pools. When comparing the PRISM climate data to the weather station data, it was found to be in general agreement (Figures 10 & 11). Furthermore, calibration values for the pools were found to be more realistic using the PRISM dataset. For example, the Coyote Springs best-fit model calibration using PRISM data predicted the soil depth to be 0.33 meters. The t-post that the weather station was attached to was hammered to the duripan and was measured to be 0.37 meters deep. After the comparisons were made, the calibration parameters from the PRISM dataset were used in the hydrologic model.

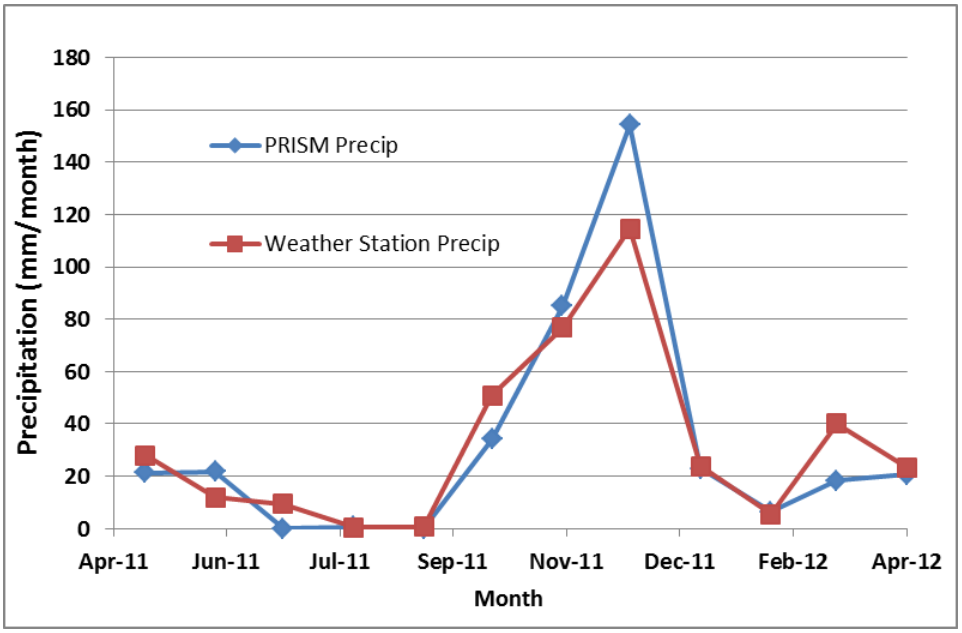

Figure 10. Comparison of monthly precipitation for PRISM and the weather station at Coyote Springs between May, 2011 and April, 2012.

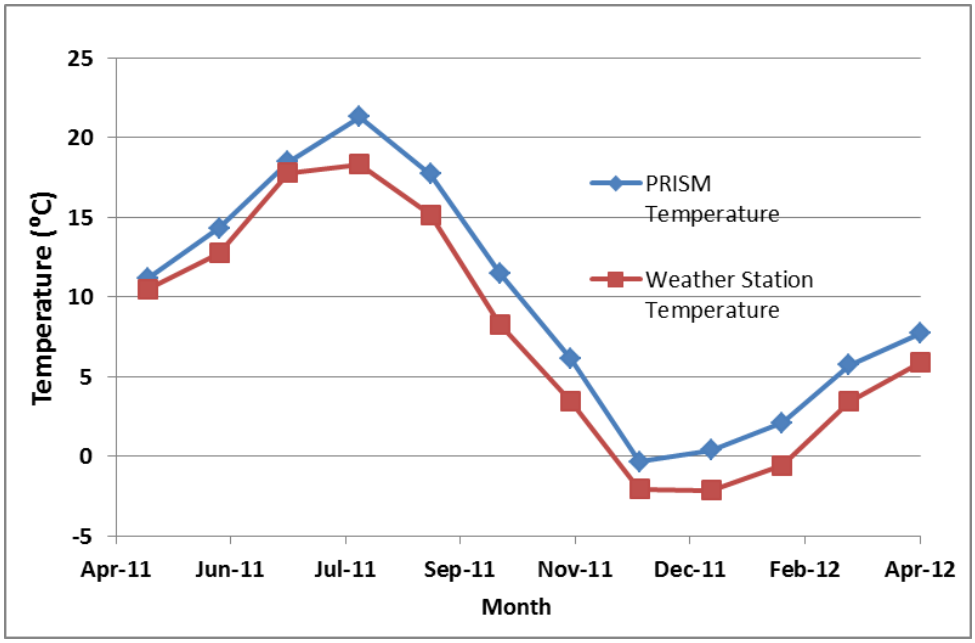

Figure 11. Comparison of average monthly temperatures for PRISM and the weather station at Coyote Springs between May, 2011 and April, 2012.

Global Circulation Model (GCM) datasets that included temperature maximum, temperature minimum, and precipitation from three models were provided by DRI. These datasets were daily bias-constructed analogs (BCCA) produced by the Canadian Centre for Climate Modelling and Analysis (CCCMA) at the University of Victoria, the Centre National de Recherches Meteorologiques (CNRM) in Toulouse, France, and the Geophysical Fluid Dynamics Laboratory (GFDL) which is operated by the National Oceanic and Atmospheric Administration in Princeton, New Jersey.

The CCCMA model is gridded with a cell size of 3.75° latitude x 3.75° longitude and a daily time-step (CCCMA, 2010). The CNRM Global Climate Model, Version 3 is gridded with cell size of 2.8° latitude x 2.8° longitude and a daily time-step (Salas-Mélia et al. 2005). The GFDL Coupled General Circulation Model Version 2.0 is gridded with cell size of 2.0° latitude x 2.5° longitude and a daily time-step (Delworth et al., 2006). The B1 and A2 scenarios were used from these three models as they are the most and least conservative of the four commonly modeled emission scenarios (IPCC, 2007). B1 is the emission scenario that assumes an aggressive emission reduction policy whereas the A2 emission scenario assumes unconstrained growth.

Because the GCM datasets are gridded to significantly larger cell sizes than the PRISM dataset, the PRISM data set was used for bulk bias correction. To bias correct temperature, mean temperature was calculated for the PRISM dataset and each GCM

dataset for the period 1980-2000. The difference between the PRISM and GCM mean temperature for 1980-2000 was added to each GCM dataset. To bias correct precipitation, mean annual precipitation was calculated for the PRISM dataset and each GCM dataset for the period 1980-2000. The difference between the PRISM and GCM mean annual precipitation was calculated as a percentage difference. The average percentage difference was applied to each precipitation value (e.g. a 20% larger mean annual precipitation value for a GCM would be corrected by dividing each precipitation value by 1.2).

The hydrologic and vegetative models were run for two ten-year time periods: 1991-2000 and 2091-2100. For 1991-2000, PRISM and each bias-corrected CCCMA, CNRM, and GFDL dataset was used for a total of four model runs. For 2091-2100, the datasets for the A2 and B1 scenarios for each bias-corrected CCCMA, CNRM, and GFDL were used for a total of six model runs (Figure 12).

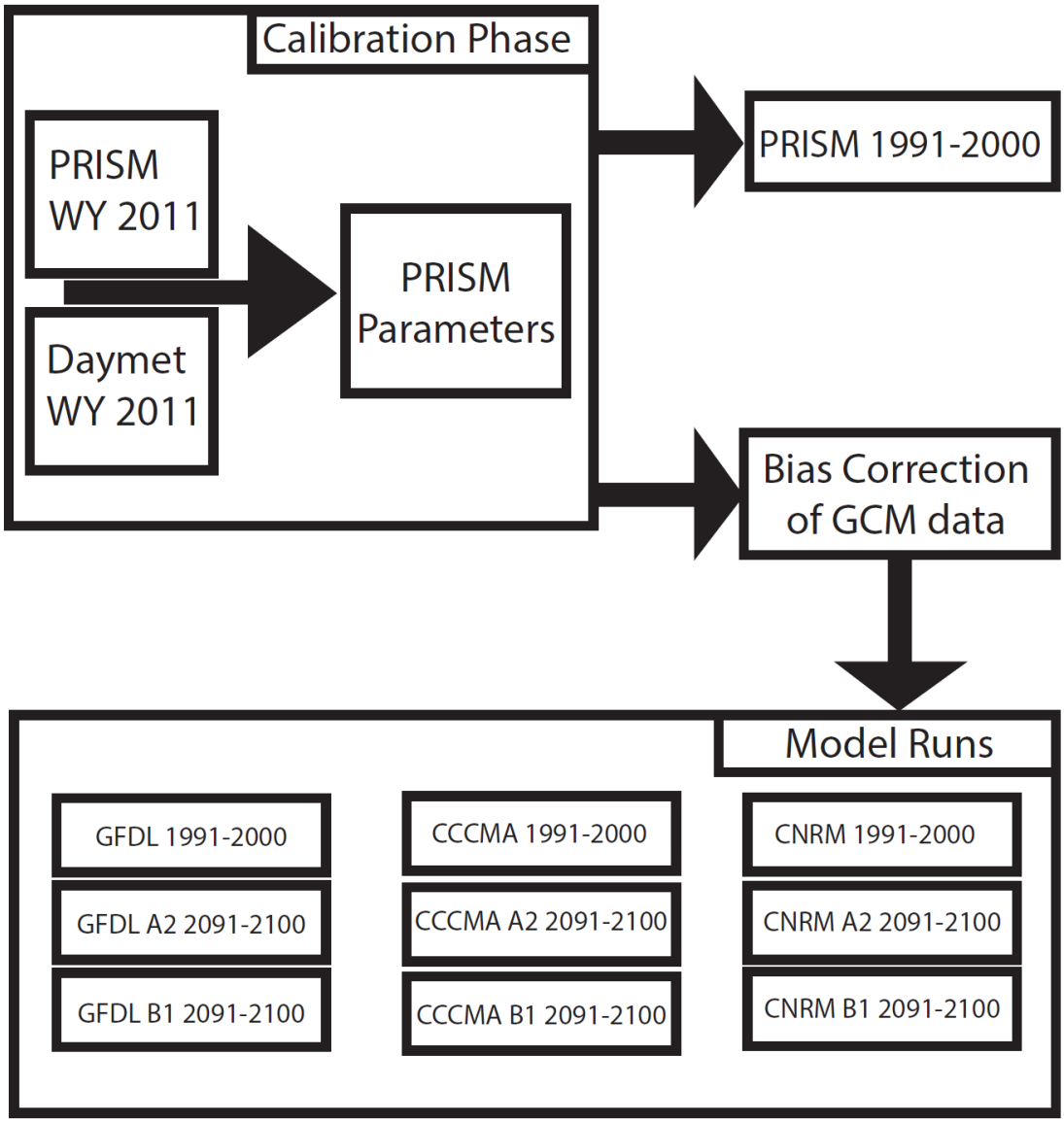

Figure 12. Flowchart representing the use of climate data

The box titled "calibration phase" shows the decision to use PRISM calibrated parameters for comparisons and to set parameter values. After parameters were selected from the PRISM calibration, the model was run using PRISM data from 1991-2000 and GCM data was bias-corrected using PRISM data. The bottom box shows the GCM data from the 1991-2000, A2 2091-2100, and B1 2091-2100 time segments that were used to run the hydrologic and vegetative models.

Hydrologic Model Development

The hydrologic model was developed in Excel 2010. It is a mass balance model with a single pool as its functional unit. Each row in the model represents a single time-step. The model is capable of running five years of climate data at a time. The model uses the solver module's evolutionary solver for non-linear and non-continuous functions to fit parameters for the model, as described in more detail in a later section of this chapter.

Hydrologic Model Spatial and Temporal Resolution

The time-step in the hydrologic model is one quarter of a month. On average, one quarter of a month is ≈7.6 days. Because we initially planned to use the publically available monthly PRISM data, this time-step was chosen as a compromise between a monthly time-step and a daily time-step, the temporal resolution of Gosejohan's (2012) vegetation inundation requirement and stage gauge data. A monthly time-step would be too coarse for determining vegetative communities within the pools. A daily time-step would be finer than appropriate for disaggregation of PRISM monthly data. The model was mostly coded by the time daily PRISM data were obtained. A large time investment would have been required at that stage to recode the model to a daily time-step, so the quarter of a month time step was left unchanged.

Data with a daily time-step, such as pool stage and climate data were aggregated into quarters of a month. The number of days in each month was divided by four (Table 3). Within each quarter, daily precipitation data were summed, and daily stage and air temperature data were averaged.

Days in a Month	Days Included in Each Quarter of a Month			
	1	**2**	**3**	**4**
31	1-8	9-16	17-23	24-31
30	1-8	9-15	16-23	24-30
28	1-7	8-14	15-21	22-28

Table 3. Assignment of days into quarters of a month for the vernal pool models

The spatial resolution of the model is controlled by the surface interpolation from the total station survey data and the stage gauge resolution. For Coyote Springs, 350 survey points were taken over an area that is roughly 46,000 m^2 for a point density of 131 m^2 per elevation point. For Adobe North, 308 points were taken over an area that is roughly 56,000 m^2 for a point density of 182 m^2 per elevation point.

Stage gauges were marked at 2 centimeter increments. To be consistent with field measurements, the hydrologic model also uses 2-cm increments for stage elevation. Stage is determined using the S:A:V relationship and the mass balance within the pool. The volume remaining in the pool after each time-step is indexed to the nearest volume in the S:A:V relationship and the associated stage is assigned to

the pool. The volume in the pool that is used for the next time step is the volume from the mass balance, not the volume associated with the stage in the S:A:V relationship.

The inputs to the hydrologic model are mean air temperature and precipitation. Mean air temperature was calculated by averaging the temperature maximum and temperature minimum for each time step for PRISM, Daymet, and all GCM datasets. Mean air temperature was calculated from the weather station data by averaging the hourly measurements. Precipitation was calculated by summing total precipitation within each time-step for all datasets.

Hydrologic Model Water Mass Balance

The components of the water mass balance within the hydrologic model fit into two broad categories: fluxes and storages. Fluxes are processes that allow water to enter and exit the system and storages are places for water to reside while in the system.

Hydrologic Fluxes

Evapotranspiration was calculated for both the soil and the open-water of the pool. Potential evapotranspiration was calculated using the Hamon (1963) simplification (Eq. 11 & 12) of the Thornthwaite method (Hamon, 1963; Thornthwaite, 1948).

$$\text{Eq 11)} \quad PET = 7.6\left\{29.8 * D * \left(\frac{e_a}{T + 273.2}\right)\right\} \quad [mm]$$

PET= Potential Evapotranspiration [mm]
D=Average Day Length for a Quarter [hours]
e_a= Saturation Vapor Pressure [kilopascals]
T=Temperature [degrees Celsius]

$$\text{Eq 12)} \qquad e_a = 0.611 * \exp\left(\frac{17.3 * T}{T + 237.3}\right) \text{ [kPa]}$$

Potential evapotranspiration was converted to actual evapotranspiration using coefficients unique to the soil and open-water (Eq. 13 & 14). These coefficients, α_{Water} and α_{Soil}, were obtained through the calibration process.

$$\text{Eq 13)} \qquad AET_{Soil} = 1000 * \alpha_{Soil} PET \quad [m]$$

AET_{Soil}= Actual Soil Evapotranspiration [m]
α_{Soil}= Soil Actual Evapotranspiration Coefficient [dimensionless]

$$\text{Eq 14)} \quad AET_{Water} = 1000 * \alpha_{Water} PET \quad [m]$$

AET_{Water}= Actual Water Evapotranspiration [m]
α_{Water}= Water Actual Evapotranspiration Coefficient [dimensionless]

The S:A:V relationship was used to calculate the evapotranspiration volume from the water, AET_{Water}, that is then multiplied by the area of the pool from the previous time-step (Eq. 15).

$$\text{Eq 15)} \quad WVE = AET_{Water} * [\text{Pool Area}_{t-1}]\ [m^3]$$

WVE=Water Volume Evapotranspiration [m^3]
Pool Area_{t-1}= Pool area from S:A:V used in the previous time-step [m^2]

To calculate the evapotranspiration from the soil, AET_{Soil} is multiplied by the maximum pool area minus the pool area from the previous time-step (Eq. 16).

$$\text{Eq 16)}\ SVE = AET_{Soil} * (\text{Max Pool} - [\text{Pool Area}_{t-1}])[m^3]$$

SVE=Soil Volume Evapotranspiration [m^3]
Max Pool= Maximum possible pool area [m^2]

The maximum pool area is defined by the area of a polygon drawn around the interface of the surrounding trees and pool basin (Fig. 4 & 5).

Precipitation volume input for each timestep was calculated by multiplying the precipitation for a quarter month by the maximum pool area (Eq. 17).

$$\text{Eq 17) Precip Volume} = \text{Precip} * \text{Max Pool Area } [m^3]$$

Precip Volume=Water Volume of precipitation [m^3]
Precip = Precipitation rate [m]

The phase of the precipitation was determined using the Water and Snow Balance Modeling System (WASMOD) method (Xu, 2002). In the WASMOD method, the phase of precipitation is a function of temperature (Eq. 18 & 19).

$$\text{Eq 18)} \quad sn_t = p_t\left\{1 - e^{[(c_t - a_1)/(a_1 - a_2)]^2}\right\} \quad [m^3]$$

sn_t=solid part of snow [m^3]
p_t=precipitation [m^3]
c_t=air temperature [degrees Celsius]
a_1=air temperature above which all precipitation is rain [degrees Celsius]
a_2= air temperature above which snowmelting begins [degrees Celsius]

$$\text{Eq 19)} \qquad r_t = p_t - sn_t \; [m^3]$$

r_t= rainfall [m^3]

a_1 and a_2 are calibration parameters for the model. a_1 is the temperature above which all precipitation is rain. a_2 is the temperature above which snow begins to melt (Xu, 2002). Rainfall enters directly into the soil and pool. Snow is added to the

snowpack (Eq. 20) and must melt before it is added to the soil and pool. The melting function is also defined by the WASMOD model as function of the a_1 and a_2 parameters (Eq. 21).

$$\text{Eq 20)}\quad sp_t = sp_{t-1} + sn_t - m_t$$

sp_t=snowpack [m^3]
m_t=snowmelt [m^3]
sp_{t-1}=snowpack from previous time-step [m^3]

$$\text{Eq 21)}\quad m_t = sp_{t-1}\left\{1 - e^{-[(c_t - a_2)/(a_1 - a_2)]^2}\right\} \quad [m^3]$$

Water can leave the system by seepage through the duripan. The seepage rate is defined as a function of stage (Eq. 23)

$$\text{Eq 22)}\ \text{Seepage} = \text{Pool Area}_{t-1} * \text{Seepage Rate}\ [m^3]$$

Seepage=seepage volume [m^3]
Seepage Rate=linear rate of seepage[m]

$$\text{Eq 23) Seepage Rate} = \text{Seepage Coeff}^{\text{Pool Stage}_{t-1}}\ [\text{m}]$$

Seepage Coeff=calibration parameter [unitless]
$\text{Pool Stage}_{t\text{-}1}$ =pool stage from previous timestep [m]

It should be noted that the term Seepage Rate (Eq. 23) has units of meters. Because this is an empirical equation, there are no units associated with the Seepage Coeff term. The Seepage Coeff is a calibration parameter in the model.

The Seepage Rate was modeled as a function of $\text{Pool Stage}_{t\text{-}1}$ for two reasons. The first reason relates to the geometry of the underlying duripan. The duripan likely tapers towards the margins of the pool basin (Figure 13). Hobson and Dalhgren (1998) found a tapering duripan in the pools they studied near Chico, CA and the pedogenic process suggests the duripan building will occur more often in lower elevations in the pool resulting in a duripan that tapers towards the margins. As the pool stage increases, the average thickness of the duripan that the pool interacts with decreases, reducing the average thickness of duripan that the water must travel through. This results in faster rates of seepage. The second reason relates to basic fluid mechanics in which the hydraulic gradient across the duripan increases as the pool stage increases.

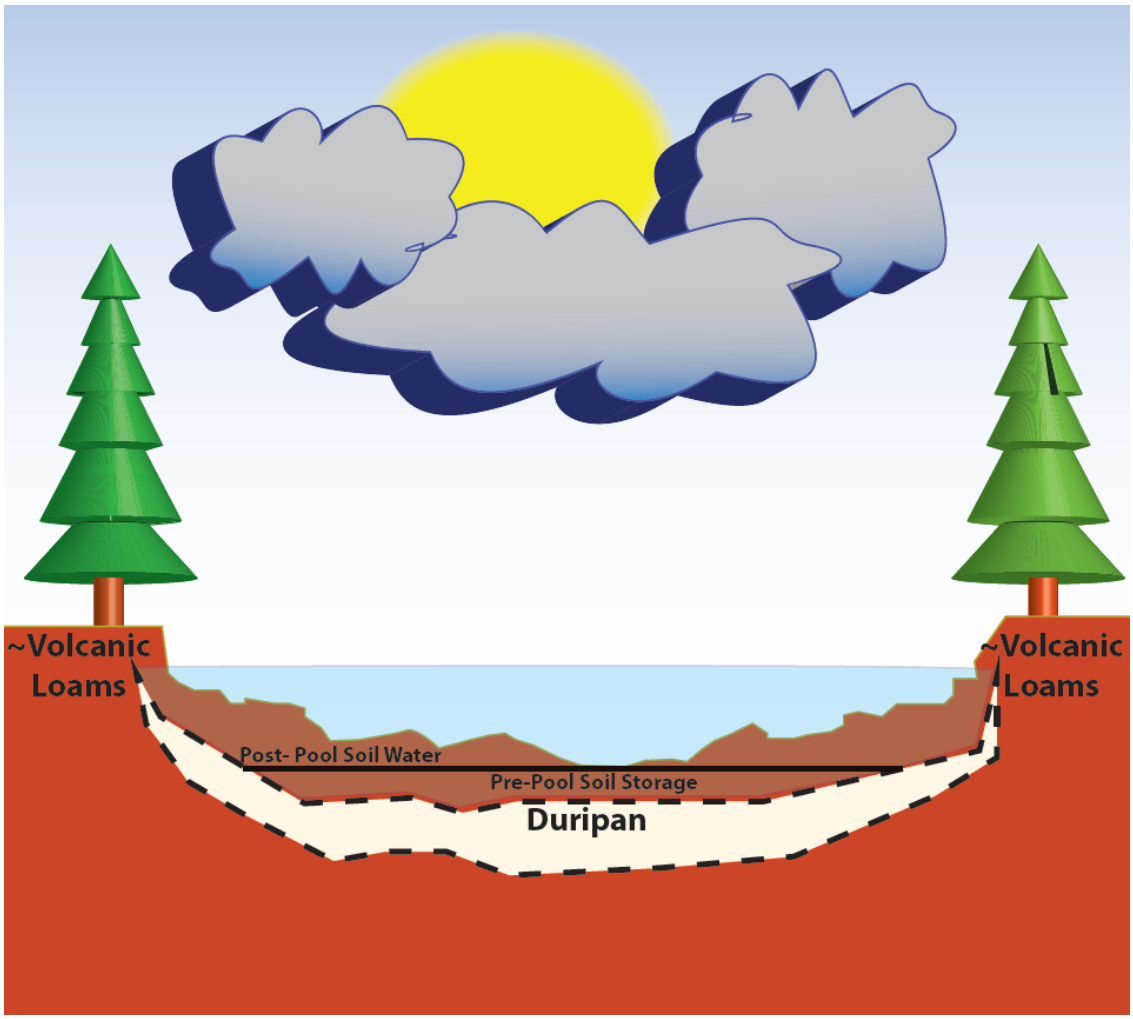

Figure 13. Conceptual diagram of volcanic vernal pools

As water enters the pool basin, soil pores below the black horizontal line must be filled before the pool is created. This storage term is called Pre-Pool Soil Storage. When the pool stage increases, water enters both the pool and soil pores above the black horizontal line. The water that enters the soil pores above the black horizontal line is a flux in the model called Post-Pool Soil Water. The duripan is thickest at the deepest part of the pool and tapers towards the margins.

When the pool stage is increased, the volume of water associated with the stage increase conceptually enters two places: the open-water pool and the unwetted soil pores above the previous depth (Figure 13). The flux of water associated with water entering the unwetted soil pores is called the Post-Pool Soil Water (Eq. 24). The partitioning of water between the pool and Post-Pool Soil Water is determined by the Basin Soil Factor and is calibrated to be a value between 0 and 1. The remaining fraction of precipitation enters the pool.

$$\text{Eq 24) Post-Pool Soil Water} = \text{Precipitation} * \text{Basin Soil Factor } [m^3]$$

Post-Pool Soil Storage=Volume of water diverted to soil when stage increases [m^3]

Basin Soil Factor=Calibrated value that partitions precipitation between soil and pool when stage is increasing [unitless]

Hydrologic Storages

Before the pool can be created, the soil pore volume between the lowest elevation in the pool basin (see the horizontal black line in Figure 13) and the duripan (Pre-Pool Soil Storage) must be filled with water. The value for Pre-Pool Soil Storage can range from zero to Pre-Pool Soil $\text{Storage}_{\text{Max}}$(Eq. 25).

$$\text{Eq 25) Pre} - \text{Pool Soil Storage}_{\text{Max}} = \text{Maximum Pool Area} * \text{Soil Depth} * \text{Porosity } [\text{m}^3]$$

Pre-Pool Soil $\text{Storage}_{\text{Max}}$=Maximum volume of storage in Pre-Pool Soil Storage [m^3]
Soil Depth=Calibrated Average depth of soil between lowest elevation and duripan[m]
Porosity=Fraction of soil volume occupied by pores[unitless]

The soil depth that is used to calculate Pre-Pool Soil Storage is a calibration parameter. Maximum Pool Area and Soil Porosity are user-specified values. Water is not routed into the pool until Pre-Pool Soil Storage is equal to Pre-Pool Soil $\text{Storage}_{\text{Max}}$.

Another water storage is snowpack (Eq. 20). Precipitation that falls as snow is added to the snowpack. Water in the snowpack does not enter the Pre Pool Soil Storage or pool until it has melted. The model assumes the water will not re-freeze.

The third water storage is the open-water pool (referred to as "the pool"). Water is routed to the pool from the Pre-Pool Soil Storage to the pool and from the pool to the Pre-Pool Soil Storage.

The fluxes of the water balance enter and exit the model through the Pre-Pool Soil Storage (Figure 13). After the model calculates the balance of the fluxes, the balance is added (positive or negative) to the Pre-Pool Soil Storage. The model then evaluates if the Pre-Pool Soil Storage is at maximum capacity. If the Pre-Pool

Soil Storage is above maximum capacity, excess water is routed to the pool. If the Pre-Pool Soil Storage is below maximum capacity, then the model either routes water from the pool back to Pre-Pool Soil Storage until it is at maximum capacity or leaves Pre-Pool Soil Storage below maximum capacity if there is no water in the pool. Figure 15 shows a flowchart for this process.

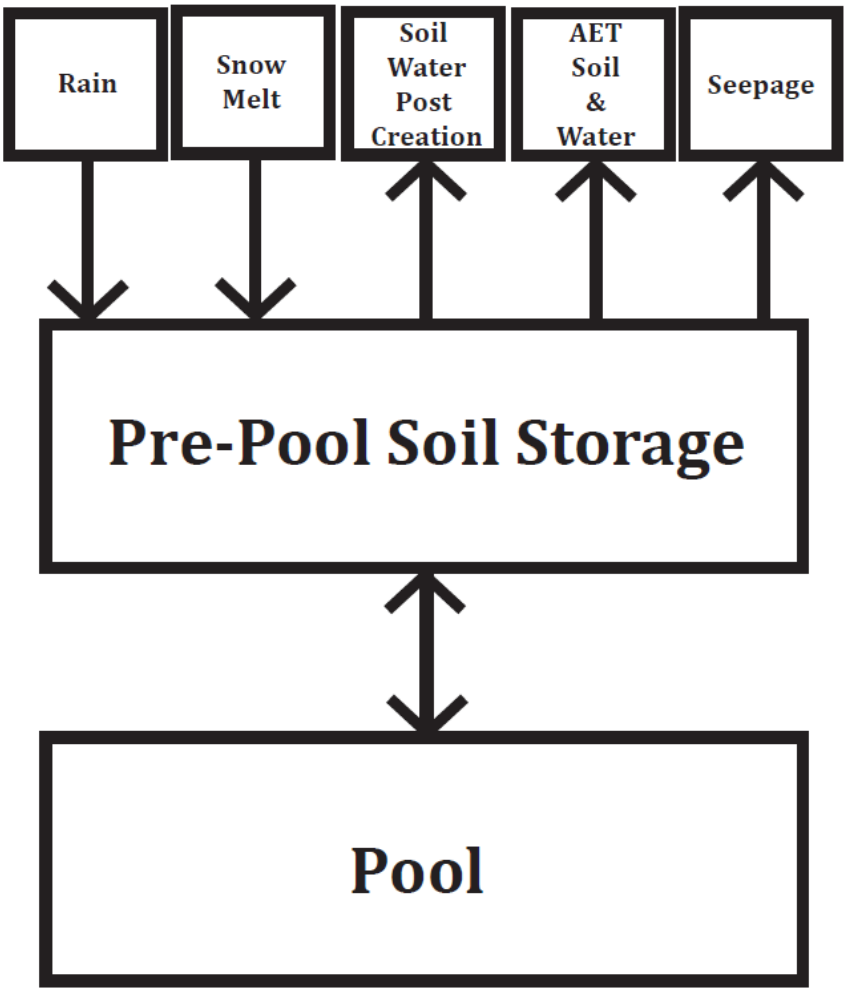

Figure 14. Conceptual diagram of water moving in and out of the system

The five boxes on top are fluxes in and out of the Pre-Pool Soil Storage. After the water balance has been calculated for a single time-step, the model puts excess water into the pool or moves water from the pool back to Pre-Pool Storage to cover water deficits. If conditions are not satisfactory for water being in the pool, no interaction between the Pre-Pool Soil Storage and the Pool occurs.

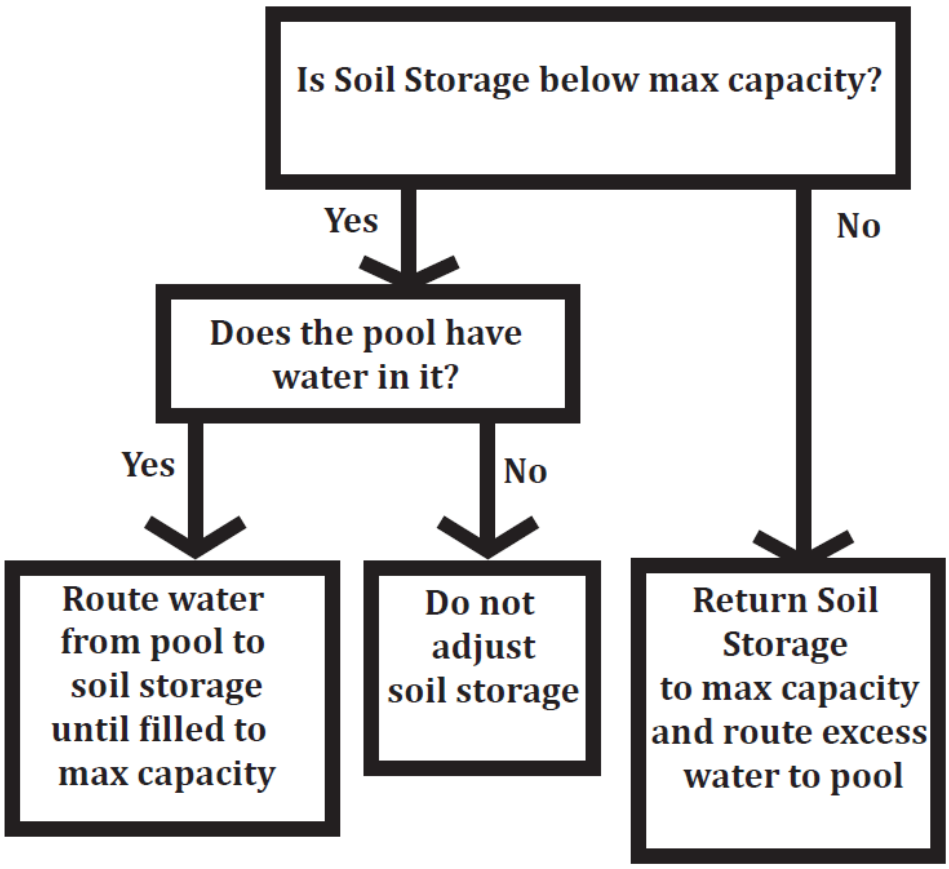

Figure 15. Decision tree that determines water routing in and out of the pool

When the Pre-Pool Soil Storage is above maximum capacity, water is always routed into the pool. If it is below maximum capacity, water is routed from the pool back to Pre-Pool Soil Storage until it returns to maximum capacity. If there is no water in the pool, Pre-Pool Soil Storage remains below maximum capacity.

While the water in the pool is ultimately what is of interest in the hydrologic model, performing the water balance in the Pre-Pool Soil Storage is simpler from the perspective of model logic. The pool is only formed when the soil defined in the

model as Pre-Pool Soil Storage is filled. Thus, to perform a water balance on the pool, the model would also have to perform a water balance on the soil to determine if conditions have been met for pool creation. Rather than having two separate water balances (one determining state for the Pre-Pool Soil Storage and one determining state within the pool), it is simpler to perform the water balance on the Pre-Pool Soil Storage and let the pool volume be a result of that water balance. This framework allows for both Pre-Pool Soil Storage and pool volume to be states within the model and allows the water balance to be calculated only once per time-step.

Pool Stage

Pool stage is ultimately what is of interest when evaluating hydroperiod and determining vegetative communities. Pool stage is determined from pool volume from the hydrologic model at the end of each time-step using an Excel lookup function and the S:A:V relationship that picks the lower value of stage when the pool volume falls between two values of volume on the S:A:V index. This provides an estimate of hydroperiod and maximum stage that are smaller than if the values were interpolated.

Calibration Metrics

The calibration metrics used for fitting the model parameters were root-mean-squared error (RMSE) (Eq. 26) and hydroperiod difference (Eq. 27).

$$\text{Eq 26) RMSE} = \sqrt{\frac{\Sigma(\text{Observed Stage} - \text{Modeled Stage})^2}{\text{Number of Observations}}} \text{ [Unitless]}$$

RMSE= Root-mean-squared error [m]
Observed Stage=Stage Observed from stage gauges [m]
Modeled Stage=Stage predicted by the model [m]
Number of Observations=Number of observed measurements

$$\text{Eq 27)Hydroperiod Diff.} = \frac{((\text{Obs. Hydroperiod} - \text{Mod. Hydroperiod})^2)^{0.5}}{\text{Obs. Hydroperiod}} \text{ [Unitless]}$$

Hydroperiod Diff.= Hydroperiod Difference [Unitless]
Obs. Hydroperiod= Hydroperiod observed from stage gauges [m]
Mod. Hydroperiod= Hydroperiod modeled [m]

RMSE is a commonly used metric that is a measure of the difference between observed and modeled values. Hydroperiod difference is a calibration metric that was created specifically for this model to penalize differences between modeled and observed pool hydroperiods. Early calibration efforts using RMSE alone resulted in

parameter values that wetted the pool later and dried the pool earlier than was observed. This disproportionately affected the deepest parts of the pool. As vernal pool specialists are typically found in the deeper parts of the pool, it is important that the parameter values selected model the hydroperiod well for this portion of the pool.

Hydrologic Model Parameter Selection

The model parameters were selected by using the solver module in Excel to minimize the sum of RMSE and Hydroperiod Difference. The evolutionary solver requires that minimum and maximum values are specified for each parameter that the solver is allowed to manipulate (Table 4).

Parameter	Units	Lower Boundary	Upper Boundary
Initial Soil Storage	m^3	0	Pre-Pool Soil Storage Max
Basin Soil Factor	unitless	0	5
AET Coeff α_{Soil}	unitless	0	1
AET Coeff α_{water}	unitless	1	2.5
Seepage Loss Factor	m/quarter	0	5
T Rain (a1)	celsius	0	5
T Snow (a2)	celsius	-100	0
Soil Depth	meters	0.1	1

Table 4. Parameters and their allowable ranges for the hydrologic model

Minimum and maximum bounds were set for each parameter within realistic ranges for use with the evolutionary solver. Pre-Pool Soil Storage Max is limited by the Soil Depth term (Eq. 25).

The ranges selected for the parameters was based on a combination of experience gained at the field sites (e.g. Soil Depth inferred from installing equipment), educated scientific opinion (e.g. α_{Water} is greater than reference ET), and WASMOD parameter specifications (e.g. a_1 is typically between 0 and 4 ^{0}C (Xu, 2002)). The range for a_1 and a_2 was set to a larger range than the WASMOD recommendations because WASMOD assumes that water is removed from the system after snowmelt and snowpack is entirely on the ground, not partially on a body of water as it is at the vernal pools. As the body of water could have some effect on the temperature values for which snow melts and precipitation phase

within the pool, these values were allowed to extend beyond the ranges specified as typical in WASMOD.

As there are eight parameters that the model is concurrently solving for, non-unique optimal parameter solutions that can exist. Furthermore, the evolutionary solver is susceptible to solving for parameter values that are local error minimums instead of finding the parameter values that yield the global minimum error. These two issues make the solver routine highly influenced by initial parameter values. To mitigate these effects, a Monte Carlo simulator was built as a macro in the Excel file.

Using the random number generator function in Excel, random non-integer values were selected from a uniform distribution of the specified range of values for each parameter. The solver function was then executed. Both the initial values and the values that the solver function converged to were then put into a summary table. This procedure was executed 200 times. The final calibrated parameter values were the values for the model run that had the smallest RMSE and Hydroperiod Difference sum of the 200 Monte Carlo runs.

Vegetation Model

There are three vegetation models per pool that use different decision trees to assign vegetative community distributions. All three vegetation models use the pool stage time-series from the hydrologic model as the only model input. Also, all

three models are based on the CART from data collected by Gosejohan (2012). The models assign vegetation community type to the area associated with each 2-cm vertical segment within the pool. The area for a given segment was calculated by taking the difference between the area associated with a given segment and the area associated with the above segment from the S:A:V relationship. As the S:A:V relationship extended into the region outside of the pool basin, the relationship was truncated in the vegetation model to predict vegetation only for the area within the maximum extent of the pool. The output of the model is the predicted area for vegetation community types defined by Gosejohan (2012) as a percentage the entire vernal pool basin.

One of the vegetation models (referred from here on as Gosejohan Combined Vegetation Model) is used for both pools as the analysis is based on the combined hydrologic and vegetation data from both pools. The decision tree used in the Gosejohan Combined Vegetation Model is from the Gosejohan (2012) analysis (Figure 6). The decision tree for the Gosejohan Combined Vegetation Model uses maximum depth and inundation length to determine plant community type. Maximum depth is unique to each elevation within the pool. Maximum depth is defined as the maximum depth of water above a given elevation within the pool. For example, if the maximum stage gauge reading for a given year was 0.24 meters, the maximum depth for the elevation associated with 0.00 meters on the stage gauge would be 0.24 meters, whereas the maximum depth associated with the elevation at 0.22 meters on the stage gauge would have a maximum depth of 0.02 meters. Thus,

the maximum depth for each 2-cm increment was calculated by taking the difference between the maximum stage gauge reading for a given year and the stage gauge reading. Inundation length was calculated by summing the number of quarters that the pool stage was above a given discretized 2-cm segment. The number for quarters was then multiplied by 7.6 days to determine days of inundation.

The remaining two models for each pool were based on pool specific hydrologic and vegetative data from Gosejohan (2012). The analysis was performed by using scripts created by Gosejohan (2012) for the CART. The additional models were created for two different reasons. The first reason is that identical plant species were found in habitats with different hydrologic conditions between Adobe North and Coyote Springs. Therefore, unique hierarchical agglomerative cluster and indicator species analyses for each pool better reflects the differences in plant community type found at each pool. The second reason for creating additional models is that Gosejohan's (2012) hierarchical agglomerative cluster and indicator species analyses is based on the hydrologic variables maximum depth and inundation length. Considering that Gosejohan's (2012) analysis was based on the assumption of equal water elevations at a given time around the pool, maximum depth and inundation length are highly related variables. Thus, if one were to look at two arbitrary points within the pool, the point with a longer inundation length would also always have a larger maximum depth. However, maximum depth and inundation length are not simply multiple scalars of each other as pool stage can

exist at a given depth for more than a single quarter. As a result, these two variables look more independent statistically speaking than they are in physical reality. Therefore, CART was performed to create a decision tree that considered only one variable at a time, either maximum depth or inundation length, for each pool. Thus, Coyote Springs and Adobe North each have three vegetation models: the Gosejohan Combined Vegetation Model (Figure 6), a unique maximum depth model (Figures 16 & 17), and a unique inundation length model (Figures 18 & 19). Validation statistics for the CART are presented in Table 5.

Plant Community Type	Weisberg Depth Coyote Springs	Weisberg Hydroperiod Coyote Springs	Weisberg Depth Adobe North	Weisberg Hydroperiod Adobe North
Short-term inundated			0.72	0.72
Edge	0.98	1.00	0.7	0.71
Shallow tolerant	0.66	0.60	0.68	0.67
Deep tolerant			0.76	0.75
Long-term inundated	0.89	0.89		

Table 5. CART validation statistics for each vegetation community model.

Maximum depth and inundation length were calculated from the hydrologic model for all of the vegetation models in the same manner as described for the Gosejohan Combined Vegetation Model.

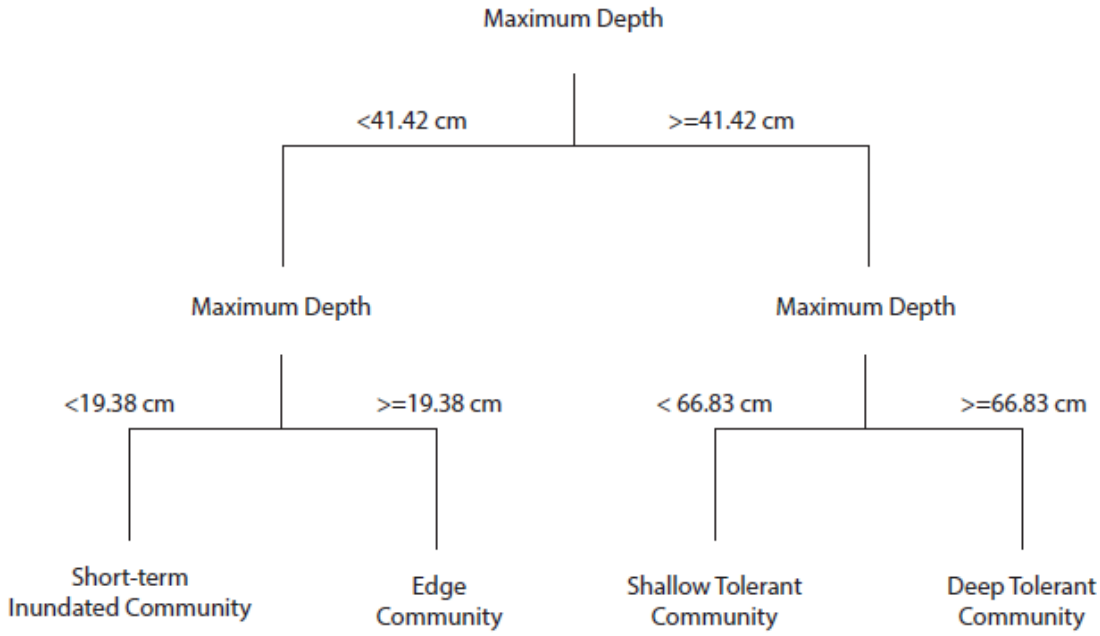

Figure 16. Adobe North vegetation model decision tree from Weisberg Maximum Depth analysis

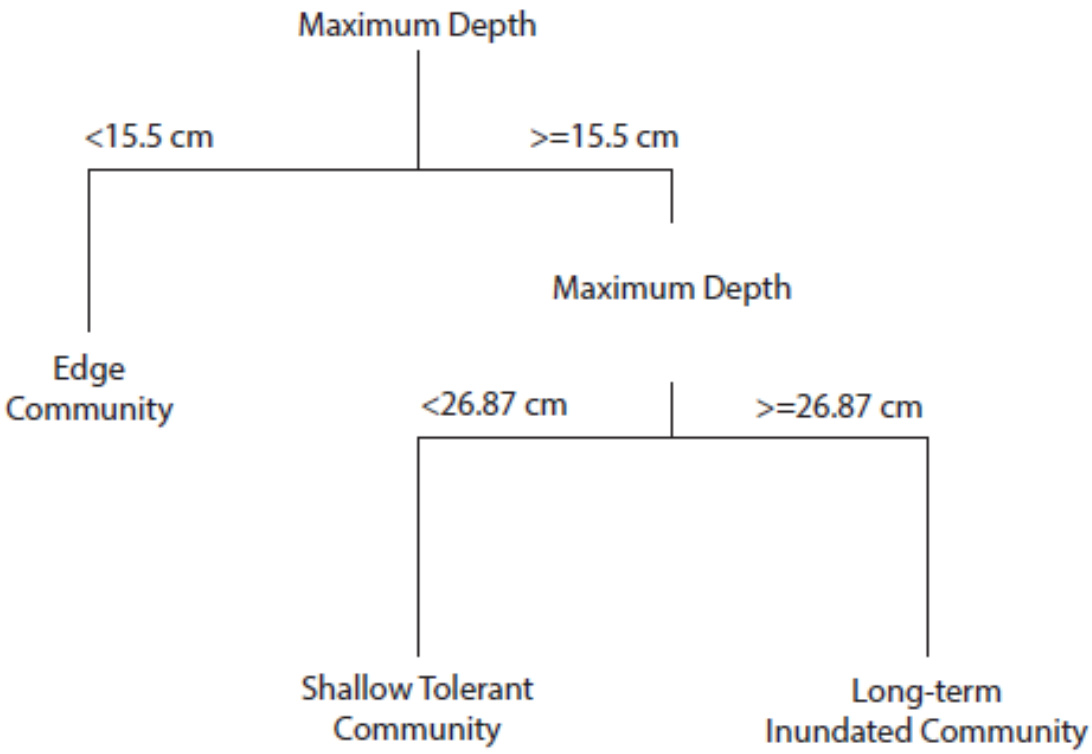

Figure 17. Coyote Springs vegetation model from Weisberg Maximum Depth analysis

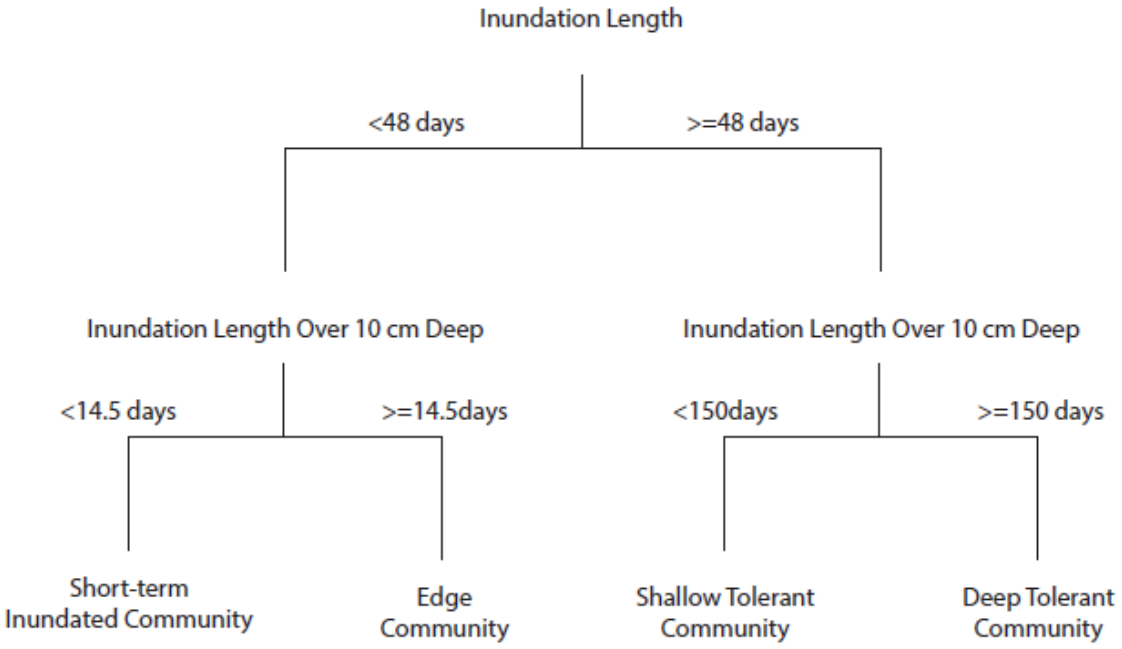

Figure 18. Adobe North vegetation model from Weisberg Hydroperiod analysis

The model considers inundation length and inundation length over 10-cm as the input variables.

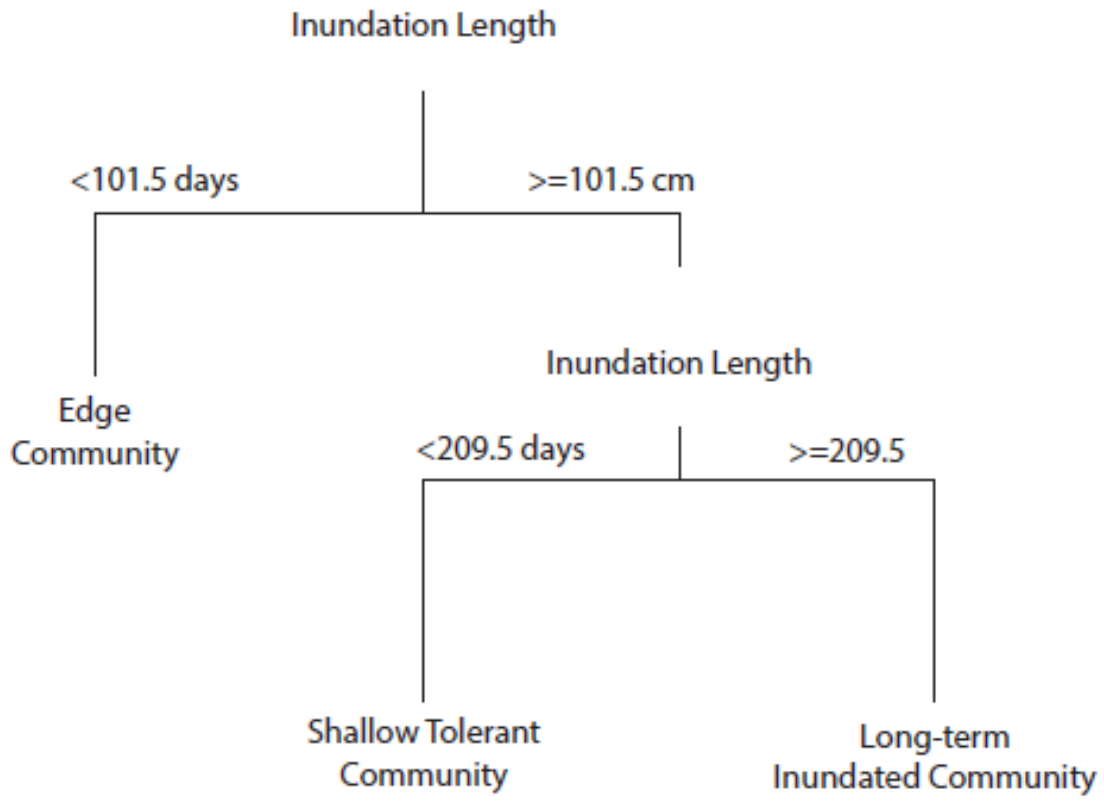

Figure 19. Coyote Springs vegetation model from Weisberg Hydroperiod analysis

Analysis

Two sample t-tests assuming equal variances were performed in Excel to determine if the means of the hydrologic model results were different between the historic and future time segments, separately for different climate change scenarios. Results from 1991-2000 were considered one sample and results from 2091-2100 were considered the second sample with each year within a given time segment considered a replicate of the time segment. T-tests for hydroperiod and maximum

depth were performed. Results of vegetation models were compared using box plots of each GCM and averages of the GCMs.

Chapter III: Results and Discussion

Soil Texture and Infiltration

Soils in Adobe North ranged from silty-clay loams at their finest and silt loams at their coarsest (Table 5). The range of soil textures in Coyote Springs was slightly coarser than in Adobe North with loam being the finest and sandy loam being the coarsest (Table 5). The average hydraulic conductivity for each pool was quite similar with Adobe North at $2.75x10^{-2}$ cm/sec and Coyote Springs at $2.67x10^{-2}$ cm/sec.

Infiltration rates were higher in the Adobe North main section, the section that was wet in April, 2012, than in the northeast arm, the section that was dry in April, 2012 (Figure 9). The Adobe North main section had an average infiltration rate of $3.49x10^{-2}$ cm/sec while the northeast arm had an average infiltration rate of $1.27x10^{-2}$ cm/sec. It may seem counter-intuitive that an area with a higher infiltration rate would stay wet for a longer period of time until one considers the soil profile and pedogenesis of the pools. As a soil profile subject to ferrolysis develops, it becomes coarser at the surface and finer at depth while developing a thicker duripan (Hobson and Dahlgren, 1998). As these soils develop, their hydraulic conductivity decreases because of duripan building.

Site Name	Abbreviations	USDA Texture Triangle	Phillip's K (cm/s)	Dingman (2002) K (cm/s)
Adobe North	Main Section_1	Silty Clay Loam	2.02E-02	1.76E-04
Adobe North	Main Section_2	Silty Clay Loam	5.55E-02	1.76E-04
Adobe North	Main Section_3	Silty Clay Loam	1.71E-02	1.76E-04
Adobe North	Main Section_3b	Silty Clay Loam	4.69E-02	1.76E-04
Adobe North	northeast_arm_1	Silt Loam	1.53E-02	7.20E-04
Adobe North	northeast_arm_2	Silt Loam	1.01E-02	7.20E-04
Coyote Springs	South_1	Loam	2.40E-02	6.95E-04
Coyote Springs	South2	Loam	4.06E-02	6.95E-04
Coyote Springs	Middle	Sandy Loam	2.25E-02	3.47E-03
Coyote Springs	North	Sandy Loam	1.95E-02	3.47E-03

Table 6. Summary of soil texture and estimated hydraulic conductivity

Hydraulic conductivity estimated using the Phillip's method. Also presented is hydraulic conductivity for a given soil texture from Dingman (2002).

There is no definitive answer as to why the northeast arm of Adobe North has different soils and infiltration rates than the main section. One possibility is related to land use within the pool. There is a man-made berm that runs north to south along the western edge of the pool (Figure 20). The origin of the soil used to create the berm is unknown. It is possible that it was disproportionately sourced from a single region of the pool which resulted in soil heterogeneity. It is also possible that if the soil was sourced from the northeast arm of the pool that the duripan was broken during the excavation process. A broken duripan could increase seepage rates by orders of magnitude. It is also possible that the main section developed

into a vernal pool earlier than the northeast arm and can be considered separate from the northeast arm despite the appearance of being a single continuous pool. It is possible that the berm was created to make the pool in the main section deeper as it confines it to a smaller area. With the main section rising to higher stage values, the northeast arm would possibly flood more often as the two sections become hydrologically connected more often. This would also explain why the northeast arm's duripan is developed less than the main section's.

Figure 20. Standing on top of the berm in Adobe North looking south. The main section is on the left. This was likely created to induce deeper pool depths for cattle by restricting the pool area.

The soils in Coyote Springs were finer in the northern portion than in the southern portion (Table 5). Similar to the trend found in Adobe North, coarser soils exhibited slightly slower infiltration rates. It should be noted that sandy loams have slower infiltration rates than loams on average, therefore Coyote Springs is not unusual in this regard (Dingman, 2002).

Overall, the infiltration rates for Adobe North and Coyote Springs were surprisingly high given their soil texture classes. In general, infiltration rates were found to be two orders of magnitude higher than the average rates for a given texture class found in Dingman (2002) (Table 5). This may be related to the ink-bottle effect as the soil pore sizes taper vertically which could lead to higher than average infiltration rates. This effect is magnified when soils are dry, as the soil matric potentials are inversely proportional to soil water content (Hillel, 1998). These infiltration tests were performed in the summer during extremely dry conditions, which would have magnified the ink-bottle effect.

Also, it should be noted that infiltration rates estimated from the tests should not be considered indicative of seepage rates through the duripan. The scale of infiltration tests (a single liter of water) cannot really simulate saturated conditions in the pool. Thus, effects of the duripan and the associated lower hydraulic conductivity are not observed in the tests. Instead, the tests are indicative of the infiltration rates near the surface for initial wetting during dry soil conditions.

Unpublished data (Iubelt, University of Nevada) has found no statistically significant difference between the hydraulic conductivity of grazed and ungrazed vernal pools in the nearby Modoc National Forest using the same infiltration test as was used in this project. The infiltration test employed in Iubelt's research and this project were testing surface soil hydraulic conductivity, not the entire integrated soil column, so the effects of compaction on seepage rates out of the pool were not actually tested. While cattle grazing may affect volcanic vernal pool hydrology (cattle using water) and vegetation (selective grazing pressure and trampling effects), it is unlikely to do so from the perspective of soil compaction. The duripan controls the pool creation and has a hydraulic conductivity that is orders of magnitude lower than the surface soil. Given the scale of infiltration rates relative to the time-step in the model and depth of soil, reductions of infiltration rates by 50% still result in the pool filling in less than a single time-step. Thus, it was not possible to use the model to test the suggestion by Marty (2005) that soil compaction by cattle in vernal pools has the potential to reduce infiltration rates and possibly result in longer hydroperiods.

Calibration Results

The parameter values for the hydrologic model that produced the smallest amount of error for Coyote Springs yielded an RMSE + Hydroperiod Difference of 0.025 meters (8.9 % of maximum depth) and an R squared value of 0.962 (Table 6

and 7). Considering the coarseness of the model's time-step and the uncertainties associated with the input data, the amount of error was determined to be satisfactory (see appendix for Monte Carlo simulation results).

Parameter Name	**Calibrated Value**	**Units**
Initial Soil Storage	2257	m^3
Basin Soil Factor	0.26	unitless
AET Coeff α Soil	0.15	unitless
AET Coeff α water	1.01	unitless
Seepage Loss Factor	2.98	unitless
T Rain (a1)	3.7	degrees Celsius
T Snow (a2)	-10.8	degrees Celsius
Soil Depth	0.334	meters

Table 7. Calibration parameters for Coyote Springs

The parameters are from the run that resulted in the smallest value of RMSE + Hydroperiod Diff. of the 200 Monte Carlo simulations.

Parameter Name	**Calibrated Value**	**Units**
RMSE + Hydroperiod Diff.	0.025	m
RMSE	0.025	m
Hydroperiod Difference	0	unitless
R squared	0.962	unitless

Table 8. Performance metrics from Coyote Springs using best-fit parameters

The performance metrics are from the run that resulted in the smallest value of RMSE + Hydroperiod Diff. of the 200 Monte Carlo simulations.

The model errors were larger for greater pool depths. At greater pool depths, the model frequently under-estimated pool depth (Figure 22). Not only was the difference between the observed stage and modeled stage greatest when the pool stage was higher, but the modeled stage alternated between increasing and decreasing pool stage more often than the observed pool stage at deeper values (Figure 21). This destabilization near the upper pool stages is likely the result of the non-linear seepage rate. As the seepage rate is a function of depth (Eq. 23), it increases exponentially with stage. While this caused some destabilization near the upper stage values, it was overall a much closer fit than modeling the seepage value linearly.

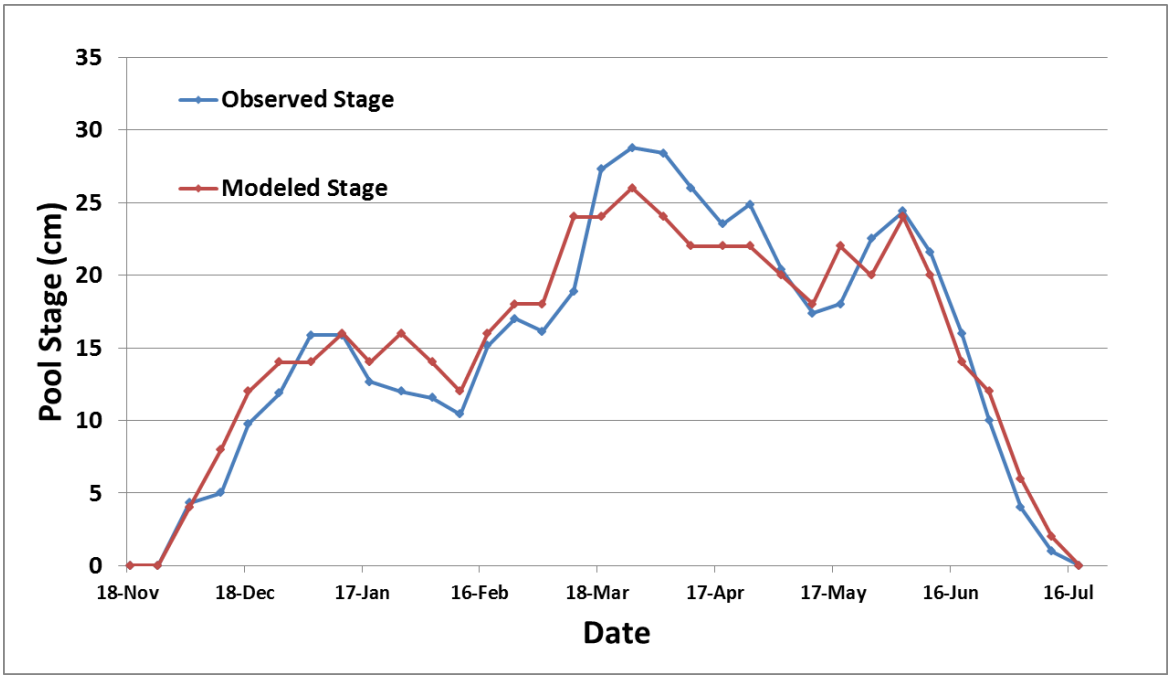

Figure 21. Modeled and observed pool stage in Coyote Springs for WY 2011

The model frequently over-estimated the pool stage in the 10 cm to 20 cm range of pool depths (Figure 22).

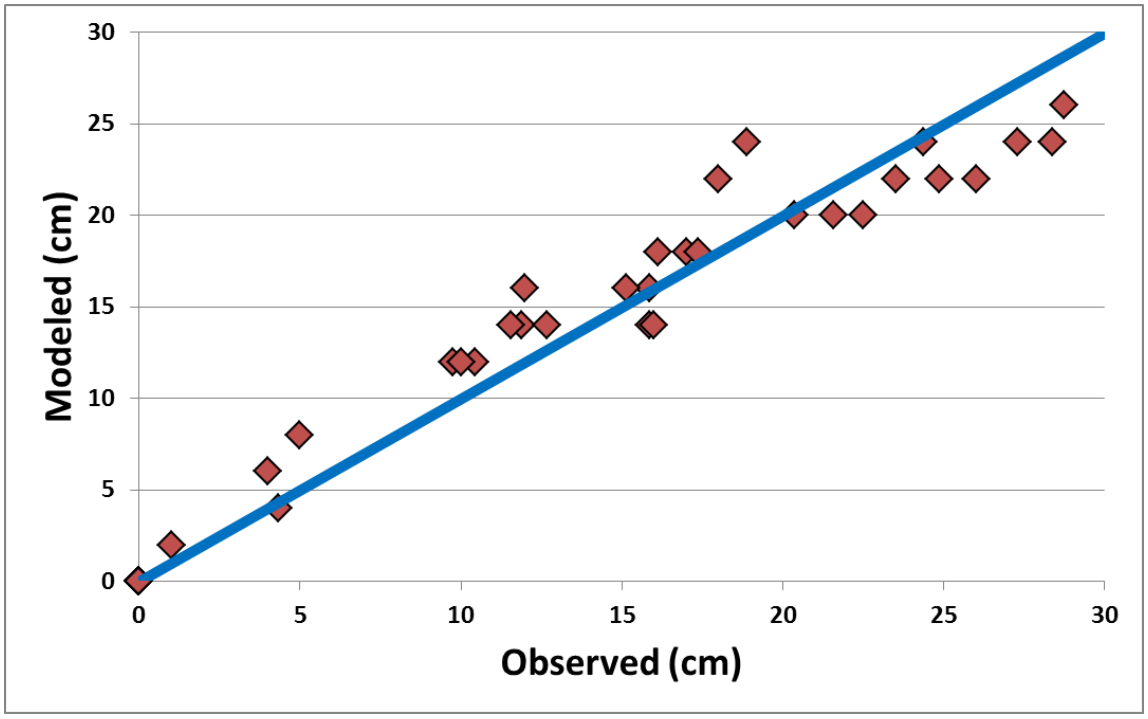

Figure 22. Comparison of observed and modeled stage for Coyote Springs for WY 2011

The line indicates model predictions aligned exactly with observed pool stage. The deviations of the diamonds from this line represent model error. The model under-predicts stage at deeper stages and over-predicts stage in the middle range of stage.

The initial soil storage that the model calibrated for, 2257 m^3, was relatively low in comparison to later runs for historical and future model runs. This may be a

result of calibrating to stage gauge readings that did not cover the entire water year. When Gosejohan (2012) installed the stage gauges in early December 2010, the pool had already formed and may have been present for a considerable amount of time before installation of the stage gauges. However, the model assumed that pooling had not begun before December because there were no stage gauge measurements before December. Thus, a low initial soil storage may have been necessary so that a larger amount of water would enter the soil before pool creation. The larger amount of water needed to enter the pool would delay pool creation until early December.

The α_{water} calibration value of 1.01 is nearly the same as the reference ET value, which is based on alfalfa evaporation which may be appropriate because of forest shading. Many of the trees that surround the pool are over ten meters tall and block direct sunlight from reaching the pool for much of the day.

The calibration value for a_2 (T snow) of -10.8 ^{0}C is lower than the range of values suggested by Xu (2002). The a_2 value is the temperature at which snow begins to melt. However, one must consider that the WASMOD model was created for use in estimating streamflow, so ponding is not a condition of the model. The presence of the liquid pool creates a large thermal mass that is above the freezing temperature. The thermal momentum of the water body results in snow melting even when the air temperature is below freezing. As there are no methods for estimating snowmelt on an open-water surface using only air temperature, the WASMOD method was selected.

When un-installing the t-post that the weather station was attached to, the soil depth was measured to be 0.37 meters. While this is only a single measurement of soil depth, it compares favorably to the calibrated soil depth of 0.33 meters.

The parameter values for the hydrologic model that produced the smallest amount of error for Adobe North yielded an RMSE + Hydroperiod Difference of 20.759 meters and an R squared value of 0.505 (Table 9). One possible reason that the model worked so poorly for Adobe North is that the seepage in the model inadequately replicated the seepage within Adobe North. When looking at the observed stage gauge measurements, there is a large and rapid increase and similarly large and rapid decrease in the last half of March (Figure 23). The scale and swiftness of the stage decrease suggests that the seepage rate is being inadequately represented in the model. Considering that the model loses water through evaporation and seepage, evaporation could not account for such a large loss of water in early spring while temperatures are still low.

Parameter Name	Calibrated Value	Units
Initial Soil Storage	2534	m^3
Basin Soil Factor	0.41	unitless
AET Coeff α Soil	0.71	unitless
AET Coeff α water	1.25	unitless
Seepage Loss Factor	3.25	unitless
T Rain (a1)	1.1	degrees Celsius
T Snow (a2)	-76.1	degrees Celsius
Soil Depth	0.294	meters

Table 9. Calibration parameters values for Adobe North

The parameters are for the run that resulted in the smallest value of RMSE+Hydroperiod Diff. of the 200 Monte Carlo Simulations.

Parameter Name	Calibrated Value	Units
RMSE + Hydroperiod Diff.	20.759	m
RMSE	20.625	m
Hydroperiod Difference	0.133	unitless
R squared	0.505	unitless

Table 10. Performance metrics for Adobe North using the best-fit parameters

The performance metrics are for the run that resulted in the smallest value of RMSE+Hydroperiod Diff. of the 200 Monte Carlo Simulations.

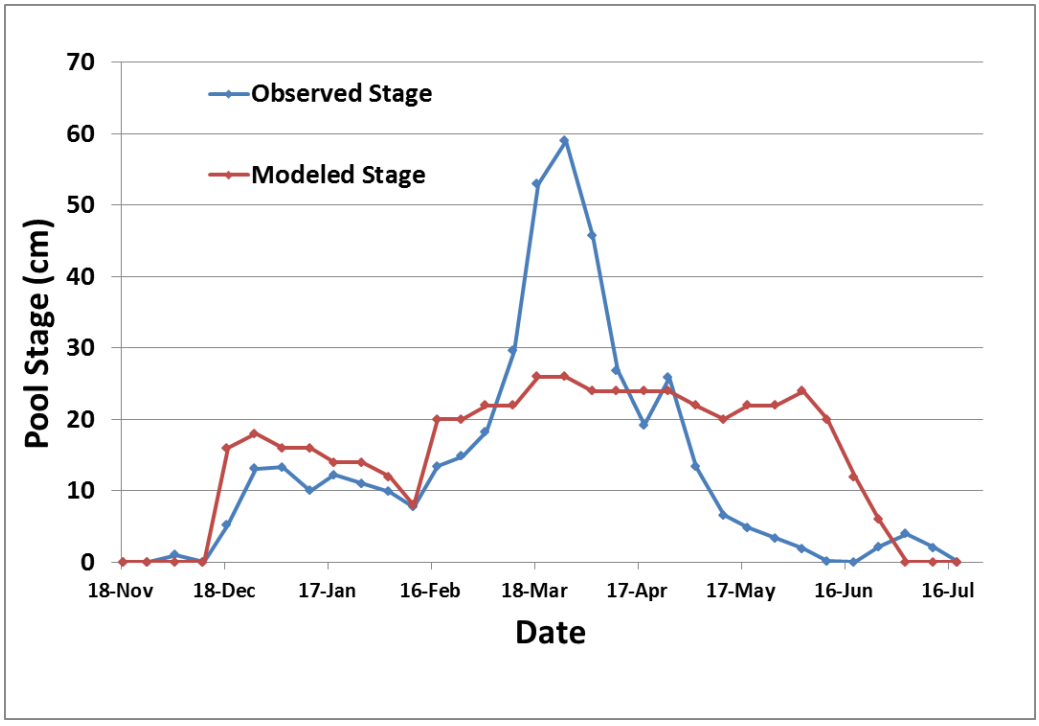

Figure 23. Modeled and observed pool stage in Adobe North for WY 2011

Best-fit calibration parameters were used and are shown in Table 7.

It is possible that seepage would best be modeled as a discontinuous piece-wise function of depth. Recalling the concept of two functionally different pools within the Adobe North basin (the northeast arm and the main section) when the pools are connected, the integrated seepage rate of the two pools (a higher seepage rate in the northeast arm than the main section) would be higher than the seepage rate within the main section alone. From the perspective of the stage gauges that were in the main section, the seepage rate would appear higher when the stage was high enough that the main section and the northeast arm are connected. At lower stages, it would appear that seepage loss was less. Furthermore, it is possible that the stage increased to a level that exceeded the elevation of the top of the duripan. This would result in an even larger increase in seepage rate as the water infiltrated into the surrounding soil that lacks a duripan to inhibit water flow. With this conceptual framework, seepage rate might be better defined by three separate piece-wise functions that increased in rate with increases in stage. As the model overestimated low values of stage and greatly underestimated high values of stage (Figure 24), this might be a satisfactory solution.

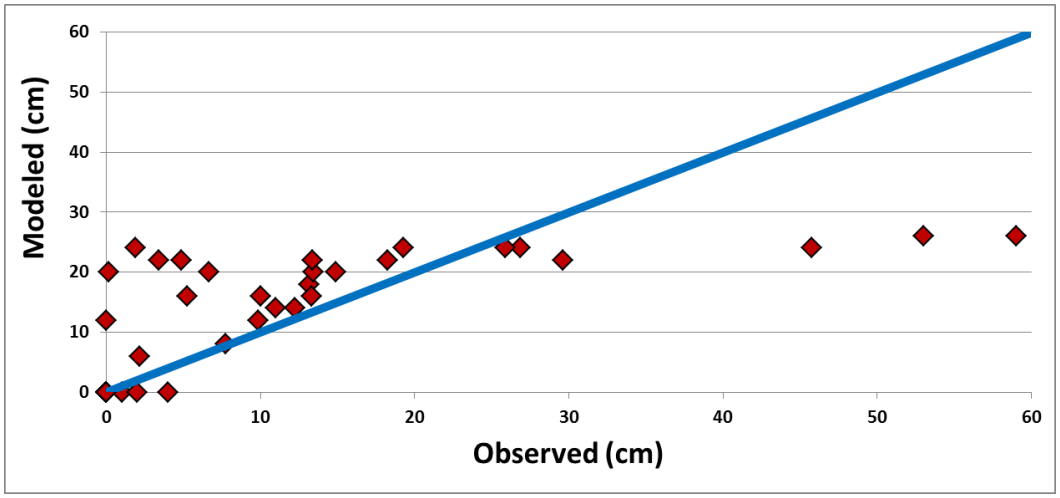

Figure 24. Comparison of observed and modeled stage for Adobe North WY 2011

The line indicates model predictions aligned exactly with observed pool stage. The deviations of the diamonds from this line represent model error. The model under-predicts stage at deeper stages and over-predicts stage in the middle range of stage.

Unfortunately, pool stage thresholds for defining the conceptual framework just mentioned are not possible with the currently available data. As such, Adobe North was not modeled for hydrology or vegetation.

Bias-Correction of GCMs

The three GCMs were quite close to each other in average annual precipitation and temperature for the calendar years 1980-2000 before bulk bias-correction (Table 8). They were less than 0.5 ^{0}C apart for temperature and within 2-cm of each other for precipitation.

Model	Average T for 1980-2000 (^{0}C)	Average Annual Precip 1980-2000 (m)	PRISM Average T for 1980-2000 (^{0}C)	PRISM Average Annual Precip 1980-2000 (m)	Bias Correction Delta T (^{0}C)	Bias Correction Precip Coeff
CCCMA	6.71	0.44	8.30	0.59	1.59	1.34
CNRM	6.73	0.46	8.30	0.59	1.57	1.27
GFDL	6.38	0.44	8.30	0.59	1.92	1.34

Table 11. GCM temperature and precipitation averages before bulk bias-correction for Coyote Springs and their corresponding bias-correction parameters

Average annual temperature and precipitation were calculated from the three climate models and PRISM for the period of 1980-2000.

After bias-correction parameters were obtained from the period between calendar years 1980-2000, the GCMs were corrected for the time periods of 1991-2000 and 2091-2100 for the A2 and B1 scenarios (Table 9). Because the bias-correction values were obtained from a longer time segment (1980-2000) than the historical segment (1991-2000), the bias-corrected average temperature and average precipitation values are not identical for the three GCMs for the 1991-2000 segment.

The GFDL precipitation for the future was considerably drier than the other two models, particularly for the A2 scenario. CCCMA temperature was the warmest model for the future scenarios.

	CCCMA		**CNRM**		**GFDL**	
Climate Segment	Temp Ave (^{0}C)	Precip (m/y)	Temp Ave (^{0}C)	Precip (m/y)	Temp Ave (^{0}C)	Precip (m/y)
1991-2000	8.0	0.62	7.7	0.55	8.4	0.60
A2 2091-2100	12.2	0.67	10.1	0.62	11.1	0.49
B1 2091-2100	9.7	0.68	9.3	0.55	10.3	0.53

Table 12. Precipitation and temperature averages for bulk bias-corrected climate data for Coyote Springs

Climate Results with Hydrologic Model

Model results for maximum depth with the GFDL and CNRM historic temperature and precipitation averages were within a few cm of the PRISM average, roughly 25 cm (Figure 25). The results for CCCMA historical were greatest at approximately 32 cm. Overall, the historical averages for maximum depth were quite close.

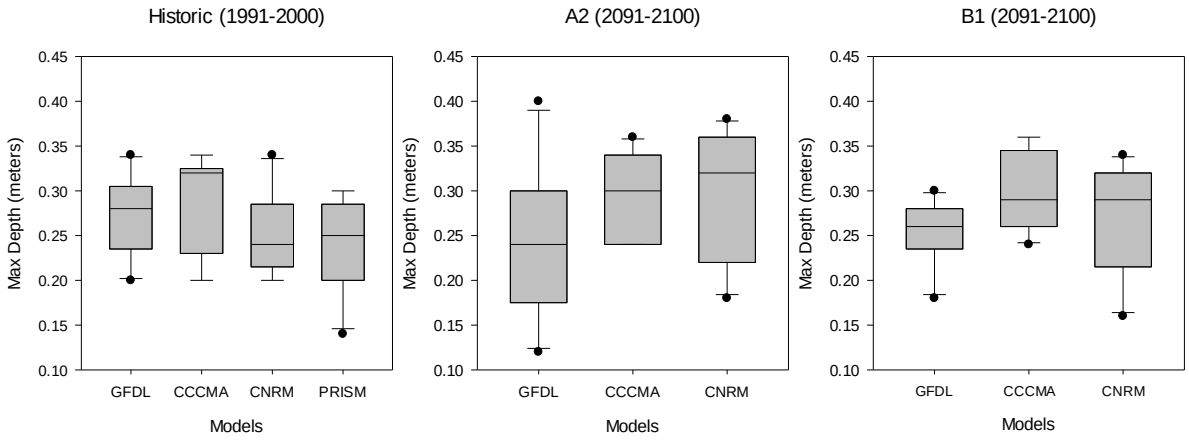

Figure 25. Box plots of maximum depth results

Maximum depth from the hydrologic model with GCM inputs by GCM for 1991-2000 and 2091-2100 for the A2 and B1 emission scenarios are shown. The historic time-period also contains a plot for model results with PRISM data.

Furthermore, there was very little change in maximum depth decadal averages for either future emission scenario (Figure 25). Somewhat surprisingly, when the three GCMs are averaged for each time-period and each emission scenario, mean maximum depth is within 0.6 cm among the historical, A2, and B1 emission scenarios (Tables 12 & 13). Thus, there is no statistically significant difference

between maximum depth results of the three GCM inputs for historical or future emission scenario for the three averaged GCM results (Tables 12 & 13).

	Historical	**A2**
Mean (m)	0.2707	0.2767
Variance	0.0010	0.0015
df	18	
P(T<=t) two-tail	0.7067	

Table 13. T-test results of maximum depth comparisons for hydrologic model outputs for averaged GCM models between historical and A2 scenarios

Results between inputs for all three GCM models for the historical (1991-2000) and A2 (2091-2100) segments are averaged by time segment. There is no statistically significant change in maximum depth between the historical and A2 emission scenarios.

Maximum depth changes insignificantly because precipitation is similar between the past and future GCM values. In addition, the precipitation continues to be concentrated primarily in the winter and late spring when temperatures are still low in the future model runs, so the pool rises to the same level.

	Historical	B1
Mean (m)	0.2707	0.2727
Variance	0.0010	0.0010
df	18	
P(T<=t) two-tail	0.8889	

Table 14. T-test results of maximum depth comparisons for hydrologic model outputs for averaged GCM models between historical and B1 scenarios

Results between inputs for all three GCM models for historical (1991-2000) and B1 (2091-2100) segments are averaged by time segment. There is no statistically significant change in maximum depth between the historical and B1 emission scenarios.

Conceptually, the maximum depth of a vernal pool within a year will be close temporally to the center of mass of precipitation. The further in time from the center of mass of precipitation, the more the water mass balance within the pool is subject to evaporation and seepage. Because the GCMs predict a similar timing and amount of precipitation in the future to what has fallen historically, the model indicates that the maximum depth within Coyote Springs is seemingly unaffected despite temperature increases in the future projections. A shift in climatic regime from a Mediterranean climate to a more dispersed precipitation pattern would likely result in decreasing maximum depths.

	A2						B1					
	Temperature (°C)			Precipitation (meters)			Temperature (°C)			Precipitation (meters)		
Month	CCCMA	CNRM	GFDL	CCCMA	CNRM	GFDL	CCCMA	CNRM	GFDL	CCCMA	CNRM	GFDL
1	3.5	1.4	3.3	1.56E-01	1.16E-01	1.02E-01	1.9	0.5	1.8	1.36E-01	9.30E-02	8.24E-02
2	5.4	3.5	5.0	1.26E-01	9.62E-02	9.93E-02	4.3	1.7	3.3	1.03E-01	8.10E-02	7.92E-02
3	6.7	5.1	7.3	6.31E-02	6.33E-02	5.25E-02	5.5	4.4	5.2	8.75E-02	4.17E-02	7.76E-02
4	8.7	8.7	9.9	3.74E-02	2.97E-02	2.31E-02	7.5	7.5	8.2	5.52E-02	3.65E-02	4.76E-02
5	13.3	14.1	13.8	2.63E-02	8.60E-03	1.13E-02	12.6	12.7	12.2	3.00E-02	9.90E-03	3.01E-02
6	17.9	19.7	20.5	9.09E-03	5.45E-03	4.12E-03	15.7	17.8	16.9	1.14E-02	3.28E-03	1.10E-02
7	23.3	22.3	25.2	2.90E-03	1.40E-03	4.76E-04	20.3	20.0	19.8	1.15E-03	1.46E-03	3.30E-03
8	22.2	21.6	23.3	2.11E-03	3.30E-03	4.60E-04	19.2	19.2	20.3	1.81E-03	2.05E-03	1.00E-03
9	19.8	18.5	19.9	3.00E-03	6.27E-03	2.93E-03	15.5	16.3	16.0	1.59E-02	2.37E-03	4.40E-03
10	13.2	13.8	12.9	3.59E-02	1.85E-02	1.84E-02	10.2	10.9	12.5	3.86E-02	3.12E-02	2.51E-02
11	6.4	6.1	8.0	7.17E-02	9.60E-02	5.74E-02	4.6	4.5	6.4	5.33E-02	1.12E-01	6.41E-02
12	3.9	2.4	3.6	1.06E-01	1.41E-01	1.02E-01	1.4	0.3	1.6	1.17E-01	1.17E-01	7.79E-02

Table 15. Average bias-corrected temperature and precipitation for the three GCMs by month and emission scenario

Model results for inundation length from historical GDFL and CCMA inputs were within five days of the results with PRISM inputs, roughly 220 days (Figure 26). Model-derived inundation length with CNRM inputs was considerably lower than the other models at roughly 200 days. The variability of PRISM inundation length was much greater than the other models. This is likely because of the difference in spatial scale between the PRISM dataset (4 kilometers) and the GCM datasets (hundreds of kilometers).

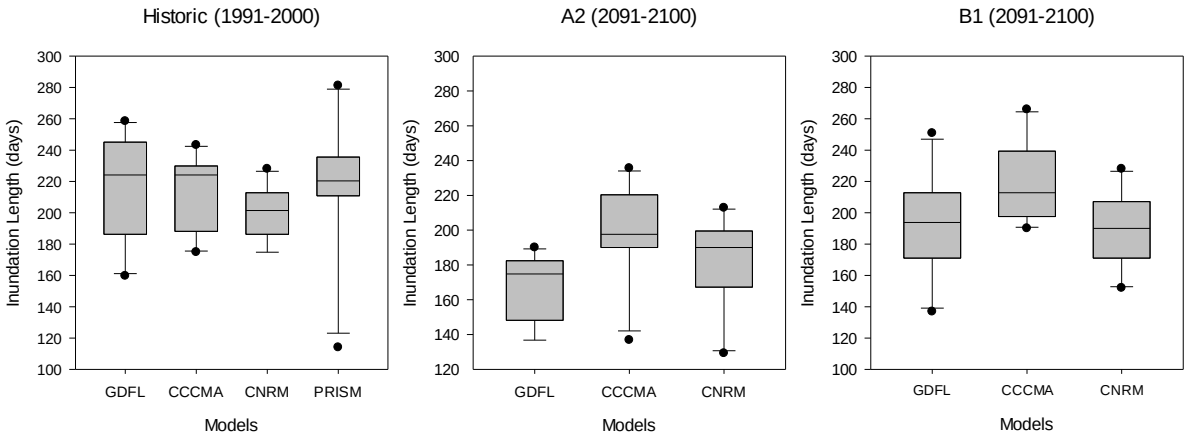

Figure 26. Box plots of hydroperiod results

Hydroperiod results by GCM for 1991-2000 and 2091-2100 for the A2 and B1 emission scenarios are shown. The historic time period also contains a plot for PRISM data.

When the hydroperiod results from the models of the three GCM inputs are averaged for each time-period and each emission scenario, hydroperiod is less for the A2 future period as compared to the historical period ($p<0.001$, $n=10$; Table 15). The average hydroperiod of 1991-2000 was 210 days while the average hydroperiod for the A2 scenario was 183 days.

	Historical	A2
Mean (days)	210.0133	182.9067
Variance	254.5005	130.9227
df	18	
P(T<=t) two-tail	0.0004	

Table 16. T-test results of hydroperiod comparisons between hydrologic model outputs for averaged GCM models between the historical (1991-2000) and the A2 simulations

While the average hydroperiod results from models with the three GCM inputs is lower for B1 (200 days) than the historical period (210 days), the change is not statistically significant (p=0.169, n=10; Table 16).

	Historical	B1
Mean (days)	210.0133	200.1333
Variance	254.5005	221.0568
df	18	
P(T<=t) two-tail	0.1691	

Table 17. T-test results of hydroperiod comparisons between hydrologic model outputs for averaged GCM models between the historical (1991-2000) and the B1 simulations

Conceptually, it appears that the climate input variables (temperature and precipitation) may have more influence on the hydrologic system at opposite times of the year. Precipitation dominates the system during the winter and spring when

temperatures are low while temperature dominates the system during the summer and fall when precipitation is low. Hydroperiod, unlike maximum depth, is affected by both mean annual precipitation and mean annual temperature. Less water and higher temperatures can each result in shorter hydroperiods. The increase in temperature for the A2 scenario is more pronounced than it is for the B1 scenario. This is likely the reason for a larger decrease in average annual hydroperiod.

Between hydroperiod and maximum depth, maximum depth is most likely to be affected by a change in phase of precipitation as precipitation that falls as snow does not enter the system until it has melted. As such, precipitation that falls as snow could affect the temporal concentration of precipitation entering the pool. The a_2 parameter, or temperature at which snow begins to melt, is much lower than temperatures observed and interpolated historically at the pool. A low value for a_2 results in snow melting quickly. Within the model, even at historic temperatures, snow melted rapidly. This is a result of the previously mentioned thermal momentum concept. Stage gauge pictures corroborated the fast snow melt that the low calibrated a_2 parameter would imply. As the snow that does fall within the pool melts quickly, a phase shift in precipitation towards more rain and less snow would likely have little effect on either the maximum depth or hydroperiod.

Vegetation Responses to Climate Impacts

Of the five possible plant communities, all three vegetation models with GCM data predicted only long-term inundated, edge, and shallow-tolerant communities at Coyote Springs. Vernal pool specialists such as *O. tenuis* are associated with the long-term inundated plant community.

Vegetation model results for percent area of maximum possible pool area for long-term inundated community with GCM historical inputs seem to be mostly in agreement, with average results ranging between 17% and 17.7% for all three vegetation models (Figure 27). PRISM historical predictions range from 13% (Weisberg Depth) to 23% (Gosejohan). Vegetation results for both the Gosejohan and Weisberg Hydroperiod model indicate nearly twice the long-term inundated community for B1 scenarios (around 12%) compared to A2 scenarios (around 6%). The Weisberg Depth model actually predicts a 2% increase in long-term inundated community for both the A2 and B1 projections (Table 17).

In general, the Gosejohan and Weisberg Hydroperiod models predict a decrease in long-term inundated community with the decrease being more pronounced for the A2 scenario. The Weisberg Depth model predicts virtually no change for either scenario.

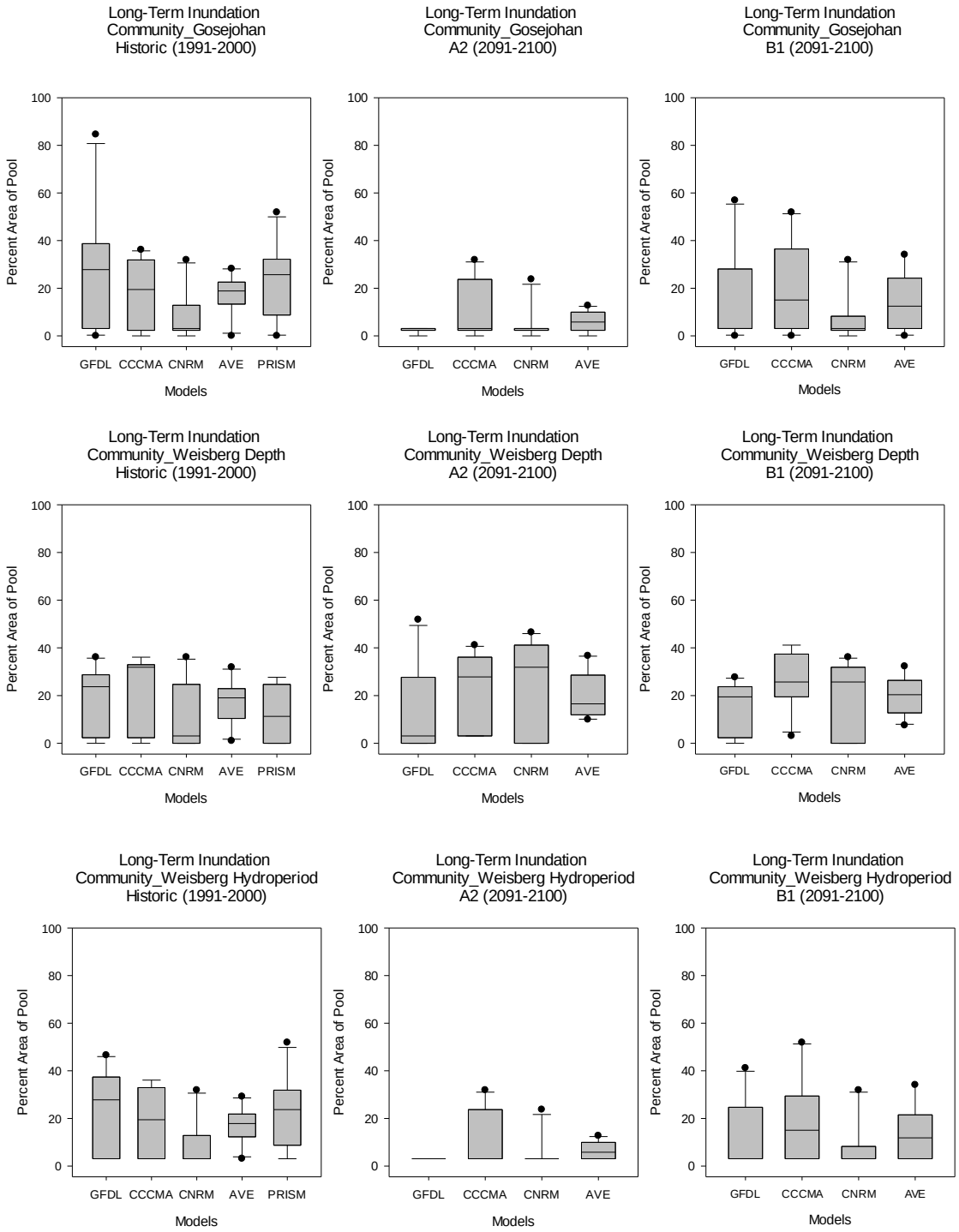

Figure 27. Box plots of long-term inundation community results

Results with GCM inputs individually as well as averaged are shown. Results are presented for models with PRISM inputs for the historical time-period as well. The graph rows are arranged by vegetation model and the graph columns are arranged by emission scenario.

The Gosejohan and Weisberg Depth models yielded identical predictions for edge community as the only difference in their decision tree was a half centimeter in their maximum depth specification (15.5 cm and 16 cm, respectively), which was less than the spatial resolution of the model (Figures 6 and 17). Both models predicted the edge community to be virtually unchanged at 56% of maximum pool area historically, 55% for the A2 scenario, and 55% for the B1 (Figure 28). Results with historic GCM values were 7% lower than those with PRISM values for the Gosejohan and Weisberg Depth models. The Weisberg Hydroperiod model predicted the edge community to be 45% of maximum pool area historically, 48% for the A2 scenario, and 43% for the B1 scenario (Figure 28). Predictions with the PRISM values were 48% and were only 3% higher than the GCM predictions for edge community.

While it is unsurprising that the two models that define the edge community by maximum depth are not changing through time considering the hydrologic model predicted no change in maximum depth in the future, it is somewhat surprising that the edge community predictions of the Weisberg Hydroperiod model showed virtually no change either. One might expect the edge community to encroach into the pool as the pool is dry for a smaller amount of time under climate change. Instead, plant community changes from the models were limited to the shallow-tolerant and long-term inundated communities.

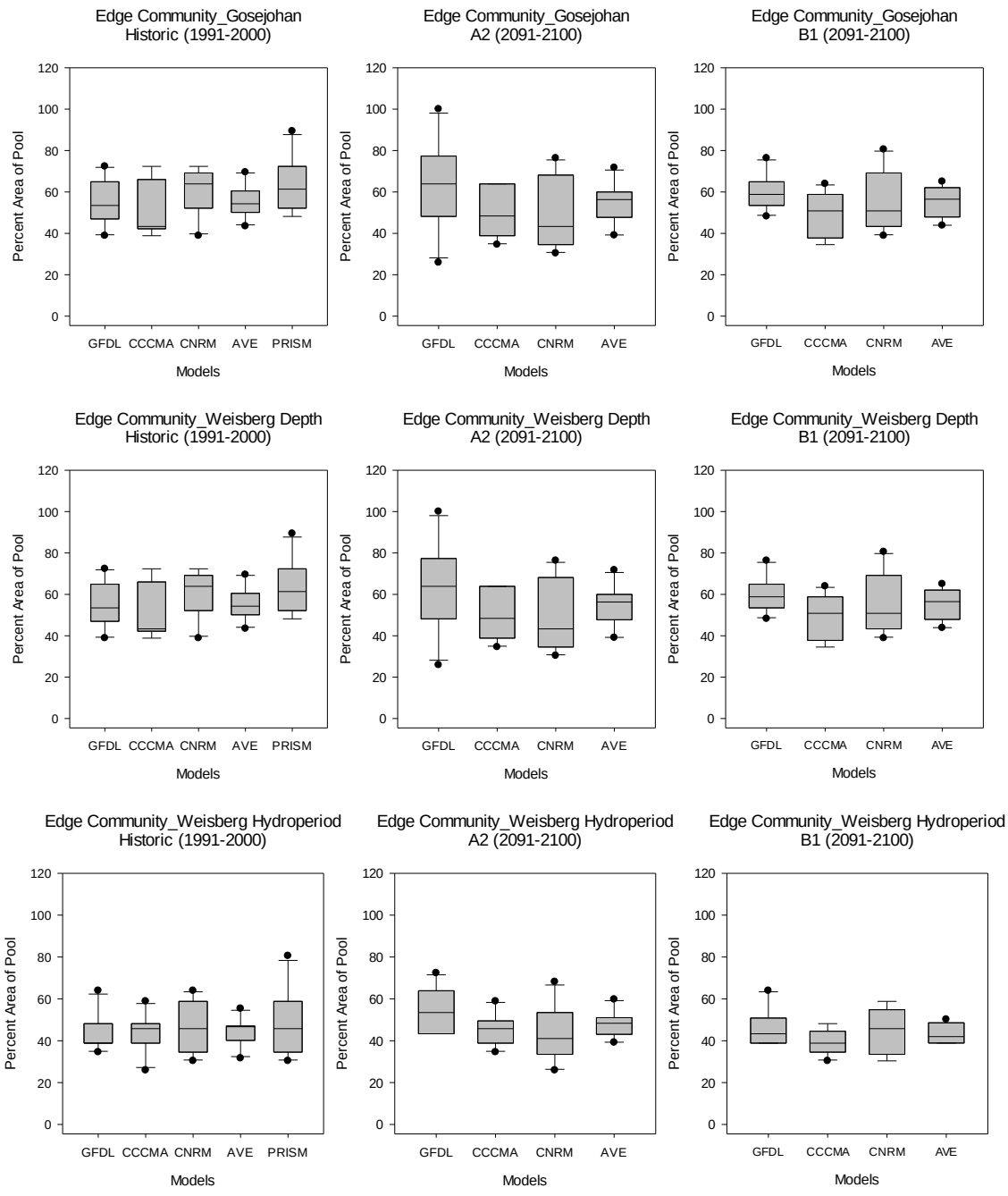

Figure 28. Box plots of edge community results

Results shown of models with GCM inputs individually as well averaged. Results are presented for the model using PRISM inputs in the historical time-period as well. The graph rows are arranged by vegetation model and the graph columns are arranged by emission scenario.

The shallow-tolerant community showed the biggest variability of the three communities among vegetation models and among GCM datasets within a given vegetation model (Figure 29). When using PRISM data, the Gosejohan model predicted 15% of maximum pool area as shallow-tolerant habitat while the Weisberg Depth and Hydroperiod models were more similar, predicting 25% and 30% respectively (Figure 29). On the other hand, when averaging the results from models with historical GCM values, the Gosejohan and Weisberg Depth model were more similar at 28% and 27% of the maximum pool area, respectively, while Weisberg Hydroperiod predicted 38% for the shallow-tolerant community. Thus, depending on the climate dataset and model used, the range for historical shallow-tolerant community ranged from 15% to 38% of maximum pool area.

When results for models with GCM inputs were averaged for predictions of shallow-tolerant community, there was an increase for the Gosejohan and Weisberg Hydroperiod models under the A2 emission scenario and a decrease in the Weisberg Depth model under the B1 scenario as compared to the historic period. The decrease in area of shallow-tolerant community in the Weisberg Depth model is only 2%. The Gosejohan and Weisberg Hydroperiod models also showed increases in shallow-tolerant area for the B1 scenario.

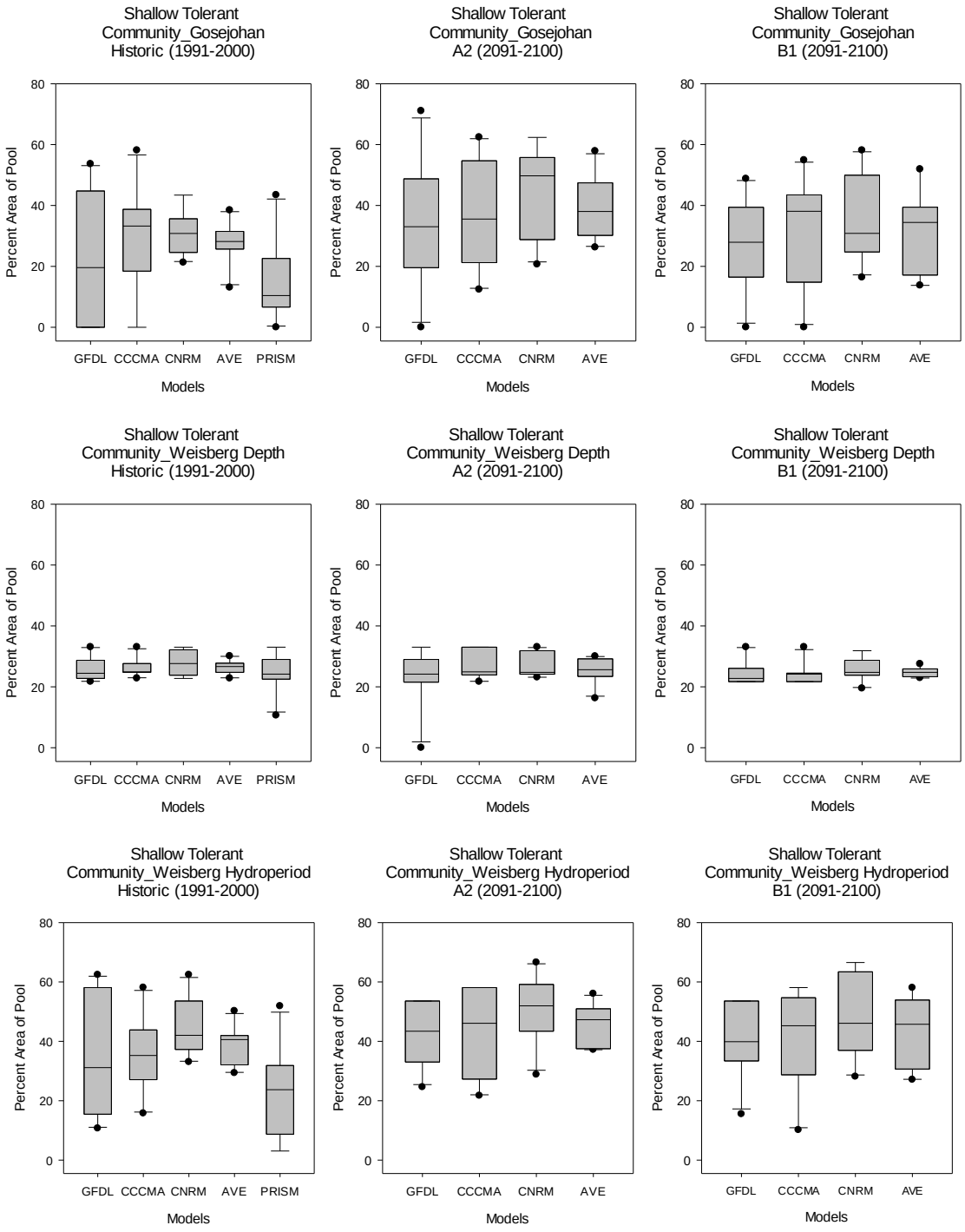

Figure 29. Box plots of shallow tolerant community results

Results shown for models with GCM inputs individually as well as averaged. Results are presented for the model with PRISM inputs in the historical time-period as well. The graph rows are arranged by vegetation model and the graph columns are arranged by emission scenario.

Overall, vegetation community types that were defined by maximum depth, such as the Weisberg Depth model and the edge community in the Gosejohan model, exhibited the least amount of change with future projections. Considering that the hydrologic model showed some changes in hydroperiod but not maximum depth, it is not surprising that plant communities defined by maximum depth would be least changed. If maximum depth actually does have ecological significance for determining plant communities, vernal plant communities will likely be more resilient to climate change.

One might have expected that climate change would push the concentric rings of plant communities from the perimeter of the pool basin inward with the edge community growing in size and the shallow-tolerant and long-term inundated communities shrinking under climate change. Instead, the models that consider hydroperiod predict that the edge community will be unchanged and under the A2 scenario, the shallow-tolerant community will acquire some of the long-term inundated community's area. This is likely related to the previously mentioned concept of precipitation dominating the system in the winter and spring while temperature dominates the system in the summer and fall. The pool is at its maximum stage early in the year while it is still cool. The edge community exists at these higher water surface elevations and is therefore influenced by increased evaporation rates for a shorter period of time. Effects of evaporation are cumulative over the entire period that the pool is wet. As evaporation rates increase as summer

approaches, the average evaporation rate observed by location in the pool increases as one moves to deeper regions in the pool. Another way of looking at the same concept is that the ratio of evaporation losses to seepage losses increases at lower elevations within the pool. As a result, hydroperiods at the lowest elevations in the pool are most affected by temperature increases.

Unfortunately, Pyke (2004), Boone et al., (2006), and Maclean et al. (2012) did not run their models using future GCM data. Comparing the hydrologic response of their models using climate forcings from different time segments to our results would be valuable to the vernal pool community.

Chapter IV: Conclusions and Recommendations for Future Work

In conclusion, this study revealed a few key points regarding hydrologic and vegetative modeling of vernal pools in the Sierra Nevada:

1. When modeling the hydrology of Sierra Nevada vernal pools, composition of the soil profile throughout the pool basin must be carefully considered. Attempts to infer physical hydrologic boundaries by topography alone are insufficient for these types of systems. The hydrologic model worked well for one pool, but the more complex hydrology of another pool was inadequately replicated.
2. Models of sensitive hydrologic systems like vernal pools require climate inputs with high spatial and temporal resolution. Daymet and PRISM climate inputs yielded very different hydrologic model outputs and calibration parameters.
3. Vegetation modeling output was very sensitive to input variable selection. Two vegetation models using different but seemingly highly related input variables, maximum depth and hydroperiod, yielded different vegetation results. Therefore, it is necessary to determine what hydrologic variables are ecologically important when modeling vegetation, which requires and improved understanding of the underlying ecophysiological mechanisms.

4. The hydrologic and vegetative models predict climate change will affect components of hydrology and the vegetative communities differently. The hydrologic model indicates no change in maximum depth but decreasing hydroperiods with increasing temperatures. The vegetative model indicates lower elevations of the pool associated with the long-term inundated plant community and vernal pool specialists to be disproportionately affected by the increasing temperatures.

While a coupled hydrologic/vegetative model is an excellent tool for quantitatively understanding the impacts of climate change on vernal pool hydrology and vegetation, the dataset that is driving the model at the time of this writing is quite limited. Thresholds of hydroperiod and maximum depth tolerance were derived from a vegetative survey paired with stage gauge observations from a single year within two pools. As the calibration was based on stage gauge readings from less than an entire water year, a longer period-of-record for the stage gauge would improve the calibration. When the stage gauges were installed in December 2010, the pools had already been created. The calibration assumed that the pools were created when the stage gauges began recording. Depending on when the pools actually formed, this limitation in the dataset would affect the parameters in the model that are assumed to be static such as soil depth.

A longer period of record could also resolve some of the stage dependent seepage rate issues that were encountered with Adobe North. Coupling a longer stage gauge record with vegetative surveys would help inform the statistical analysis that drives the vegetative models. Multiple years of coupled stage gauge records with vegetative surveys would illuminate the importance of different hydrologic variables (i.e. maximum depth, period of inundation, or perhaps other variables such as water temperature that are not considered in the model) on vegetative distributions within the pool. It is possible that hydrologic preferences are less constrained than is assumed in the model and that other factors, such as the seed bank at the plot scale, are far more important. It would also be helpful to couple a plot level soil survey with the vegetative survey. The differences in soil texture between the northeast arm and main section of Adobe North and the lack of *O. tenuis* abundance in the northeast arm (Gosejohan, 2012) suggest that soil texture could be a powerful indicator for vegetative distribution. Soil texture could also be used as proxy for soil profile development in ferrolytic soils.

Knowing the extent of the underlying duripan could also be valuable for modeling Adobe North. This could be performed by gravity or resistivity measurements or perhaps a penetrometer survey. The advantage to using gravity measurements would be that thickness of the duripan might be obtained. Ultimately, effective modeling of Adobe North would require knowing seepage rates for both the northeast arm and the main section. A simple approach would be to install a stage gauge in the northeast arm. This would allow for the seepage rate unique to the

northeast arm to be calibrated for. When used in conjunction, the threshold for pool spillage could be obtained by observing the stage at which the seepage rate exceeded the integrated seepage rates of the northeast arm and the main section.

Adobe North and Coyote Springs are functionally different than more commonly studied pools controlled by clay-rich soils. Monitoring pools with different edaphic characteristics but similar species compositions would help to differentiate the relative importance of hydrology and soil characteristics in determining vegetation distributions. It is possible that hydroperiod requirements are different in pools with finer soils because of differences in soil matric potentials affecting plants' access to water. Cation exchange capacities (CEC) can be greatly reduced in soils subject to ferrolysis (Hobson and Dahlgren, 1998). As CECs are somewhat indicative of soil fertility, different CECs could result in differing plant communities (Hillel, 1998).

As was previously mentioned, factors that are species specific besides hydrology can influence plant community structure. A coupled model that considered other variables in addition to hydroperiod and maximum depth would likely improve modeled results. Possibilities for model variables include pH, water temperature, and soil texture among others. The variable 'average depth' would be perhaps more indicative of plant community than maximum depth. Average depth might be more ecologically important to plants as it would represent what depth of water a given plant experiences while growing whereas maximum depth occurs early in the life cycle. For adjacent elevations near the pool basin perimeter where

seepage rates are faster, differences between maximum depths are smaller proportionately than differences in hydroperiod because water leaves the pool so quickly at high stage values. It is possible that these maximum depth values are ecologically insignificant if it is inundated for very short periods of time e.g. a single week.

While the vegetative models are derived from statistical analysis, they are deterministic in assigning vegetative communities. It is likely that in reality there is much overlap in vegetative community tolerance. The vegetative models also do not consider what is "optimal" hydrologically. Gosejohan (2012) found no upper threshold for hydroperiod or maximum depth in the long-term inundated and deep tolerant communities respectively. However, to function as a vernal pool and not a permanent lake, the pools must dry out which puts limits on how long they can be inundated and how deep the pools can be. Knowing what is optimal and not merely tolerable would give more clarity to the thresholds defined in the vegetative models. Furthermore, the statistical analysis that determines vegetation preferences for hydrologic thresholds are derived from open-systems with many unknown variables (e.g. grazing pressure, soil texture, seed bank composition, etc.). Determining hydrologic thresholds in a lab setting that reduces unknowns and explicitly tests for hydrologic thresholds for various plant species found in vernal pools would be preferable to a statistically inferred model.

The time-step in the model was likely a factor in determining vegetation distributions in the pool. Maximum depths were calculated from stage recordings

that were averaged over each quarter of a month. Unless the highest stage reading within the pool was the same for the entire quarter of a month, the maximum depth at the daily time-step would always be larger than the maximum depth value calculated from averaging stage at the quarter of a month time-step. Using the model at a daily time-step rather than a quarter of a month time-step would likely shift some of the vegetation communities within the pool.

The climate data that are currently driving the hydrologic model are coarse in their spatial resolution. Spatial resolution is particularly important in mountainous regions, such as where Adobe North and Coyote Springs are located, as precipitation is sensitive to topographic variation (Daly et al., 1994). A longer period-of-record of weather station data would be helpful for bias-correction of GCM data. While the PRISM dataset was helpful for bias-correcting the GCM datasets, actual weather station data that does not rely on interpolation would be preferable.

References:

Allen R.G., Pereira L.S., Raes D., Smith M., Crop evapotranspiration-guidelines for computing crop water requirements, FAO irrigation and drainage paper. Food and Agriculture Organization of the United Nations, Rome, 1998

Bauder E., Inundation effects on small-scale plant distributions in San Diego California vernal pools, Aquatic Ecology, Vol 34: pg 43-61, 2000

Bliss S. and Zedler P., The germination process in vernal pools: sensitivity to environmental conditions and effects on community structure, Oecologia, Vol 113, pg 67-73, 1998

Boone R., Johnson C. M., Johnson L. B., Simulating vernal pool hydrology in central Minnesota, USA, Wetlands, Vol. 26, No.2, pg. 581-592, 2006

Brinkman R., Ferrolysis, a hydromorphic soil forming process, Geoderma, Vol. 3, pg. 199-206, 1970

Brooks R.T. and Hayashi M., Depth-Area-Volume and Hydroperiod Relationships of Ephemeral (Vernal) Forest Pools in Southern New England, Wetlands, Vol. 22, pg 247-255, 2002

Brooks R.T., Weather-Related Effects On Woodland Vernal Pool Hydrology And Hydroperiod, Wetlands, Vol 24 No. 1, pg. 105-114, 2004

Campbell G. S., An Introduction to Environmental Biophysics, 1st Edition, Springer-Verlag, New York, NY, 1977

Canadian Centre for Climate Modelling and Analysis, http://www.cccma.ec.gc.ca/data/cgcm3/cgcm3_t47_20c3m.shtml , accessed 6/21/2013, Last Updated 5/19/2010

Cayan D., Kammerdiener S., Dettinger M., Caprio J., Peterson D., Changes in the Onset of Spring in the Western United States, Bulletin of the American Meteorological Society, Vol 82, No 3, pg 399-415, 2001

Clark M., Lis R., Fairbanks D., and Schierenbeck K., A spatial and temporal investigation of Eleocharis Macrostachya and Orcuttia Tenuis, Madrono, Vol. 55, No. 4, pg 257-268, 2008

Daly C., Neilson R., Phillips D., A Statistical-Topographic Model for Mapping Climatological Precipitation over Mountainous Terrain, Journal of Applied Meteorology, Vol. 33, pg 140-158, 1994

Delworth T.L., Broccoli A. J., Rosati A., and Coauthors, 2006 ,GFDL's CM2 Global Coupled Climate Models. Part I: Formulation and Simulation Characteristic, Journal of Climate-Special Section, Vol. 19, pg 644-673

Dettinger M. and Cayan D., Large-Scale Atmospheric Forcing of Recent Trends toward Early Snowmelt Runoff in California, Journal of Climate, Vol. 8, pg 606-623, 1995

Dingman S. L., Physical Hydrology Second edition, Waveland Press, Illinois, 2002, printed in the USA

Dufrêne, M. and P. Legendre, Species assemblages and indicator species: the need for a flexible asymmetrical approach. Ecological Monographs 67:345–366, 1997

Golden Software, User's Guide: Contouring and 3D Surface Mapping for Scientists and Engineers, Golden Software, Inc., Golden, CO, 2002

Gosejohan M., Effects of Hydrology and Livestock Use on Modoc Plateau Vernal Pool Region Plant Communities, MS Thesis of University of Nevada, Reno, 2012

Green A.T., Hobson W.A., Dahlgren R.A., Kelley D.B., Evaluation of Soil Properties and Hydric Soil Indicators for Vernal Pool Catenas in California, Wetland Soils, Vol. 23 No. 3, pg 727-740, 2008

Hamon R.W., Computation of direct runoff amounts from storm rainfall, International Association of Scientific Hydrology, Publication 63, 1963

Hillel D., Environmental Soil Physics, Academic Press, San Diego, California, 1998

Hobson W.A. and Dahlgren R.A., Soil Forming Processes in Vernal Pools Of Northern California, Chico Area, Ecology, Conservation, and Management of Vernal Pool Ecosystems-Proceedings from a 1996 conference, California Native Plant Society, Sacramento, pg. 1-14, 1998

Holland R. and Jain S., Terrestrial vegetation of California 3rd Edition, Vernal Pools, University of California Press, New Jersey, pg. 515-533, 1988

Hurt G.W. and Vasilas I.M., Field indicators of hydric soils in the United States, National Soil Survey Center, Version 6.0, Lincoln, NE, 2006

Intergovernmental Panel on Climate Change (IPCC), Summary for Policymakers, In: Climate Change 2007: The Physical Science Basis. Contribution of Working Group 1 to the Fourth Assessment Report of the Intergovernmental Panel on Climate Change [Solomon S., Qin D., Manning M., Chen Z., Marquis M., Averyt K.B., Tignor M., and Miller H.L. (eds.)]. Cambridge University Press, United Kingdom and New York, 2007

Jackson M.L., Soil Chemical Analysis: Advanced Course, Parallel Press, University of Wisconsin, Madison, WI, 2005

Jepson W.L., A manual of flowering plants of California, Associated Students Store, University of California, Berkley, CA, 1925

Keeley J.E., Photosynthesis in vernal pool macrophytes: relation of structure and function, in: Ikeda D.H. and Schlising R.A., Vernal Pool Plants: Their Habitat and Biology. Studies from the Herbarium, No. 8, California State University. Chico, CA, 1990

Keeley J.E., Anaerobiosis and fungi in the germination of two vernal pool grasses, American Journal of Botany, Vol. 75, pg. 1086-1089, 1988

Keeley J. and Zedler P., Characterization and Global Distribution of Vernal Pools, Ecology, Conservation, and Management of Vernal Pool Ecosystems-Proceedings from a 1996 conference, California Native Plant Society, Sacramento, pg. 1-14, 1998

Lin J., The floristic and plant succession in vernal pools vegetation, M.A. thesis, San Francisco State College, San Francisco, 1970

Maclean I., Bennie J. J., Scott A.J., Wilson R.J., A high-resolution model of soil and surface water conditions, Ecological Modelling, Vol. 237, pg 109-119, 2012

Marty J., Effects of Cattle Grazing on Diversity in Ephemeral Wetlands, Conservation Biology, Vol. 19, pg. 1626-1632, 2005

McLaughlin E., Autecological studies of three species of Callitriche native in California, Ecology Monographs, Vol. 44, pg 1-16, 1974

McVaugh R., The Vegetation of the Granitic Flat-Rocks of the Southeastern United States, Ecological Monographs, Vol. 13, pg 119-166, 1943

Norris R.M. and Webb R.W., Geology of California, John Wiley & Sons, New York, NY, 1976

Natural Resources Conservation Service (NRCS), Hydric soils overview, http://soils.usda.gov/use/hydric/overview.html , accessed 5/16/2013, National Resources Conservation Service

Pyke C., Simulating vernal pool hydrologic regimes for two locations in California, USA, Ecological Modelling, Vol. 173, pg 109-127, 2004

Rains M., Dahlgren R., Fogg G., Harter T., Williamson R., Geological control of physical and chemical hydrology in California vernal pools, Wetlands, Vol. 28, No. 2, pg 347-362, 2008

Salas-Mélia, D., F. Chauvin, M. Déqué, H. Douville, J.F. Gueremy, P. Marquet, S. Planton, J.F. Royer and S. Tyteca, 2005, Description and validation of the CNRM-CM3 global coupled model, CNRM working note 103

Simovich M.A., Crustacean Biodiversity and Endemism in California's Ephemeral Wetlands, Ecology, Conservation, and Management of Vernal Pool Ecosystems-Proceedings from a 1996 conference, California Native Plant Society, Sacramento, pg. 107-118, 1998

Smith D.W. and Verrill W., Vernal Pool-Soil-Landform Relationships in Central Valley, California, Ecology, Conservation, and Management of Vernal Pool Ecosystems-Proceedings from a 1996 conference, California Native Plant Society, Sacramento, pg. 15-23, 1998

Spencer S.C. and Riesberg L.H., Evolution of Amphibious Vernal Pool Specialist Annuals: Putative Vernal Pool Adaptive Traits in Navarretia (Polemoniaceae), Ecology, Conservation, and Management of Vernal Pool Ecosystems-Proceedings from a 1996 conference, California Native Plant Society, Sacramento, pg. 76-85, 1998

Stewart I., Cayan D., Dettinger M., Changes in snowmelt runoff timing in Western North America under a 'business as usual' climate change scenario, Climatic Change, Vol 62, pg 217-232, 2004

Thornthwaite C.W., An Approach toward a Rational Classification of Climate, Geographical Review, Vol 38 No 1, pg 55-94 1948

Thornton P.E., Running S.W., White M.A., Generating surfaces of daily meteorological variables over large regions of complex terrain, Journal of Hydrology, Vol. 190, pg 214-251, 1997

Thornthwaite C. W. and Holzman B., The determination of evaporation from land and water surfaces, Monthly Weather Review, Vol 67, Issue 1, pg 4-11, 1939

U.S. Department of Agriculture (USDA), Urban hydrology for small watersheds, USDA Soil Conservation Service, Engineering Division, Technical Release 55, Washington D.C., USA, 1986

Web Soil Survey, http://websoilsurvey.nrcs.usda.gov/app/HomePage.htm, 2/17/2012, USDA, accessed May 2012

Xu C.Y., WASMOD- The water and snow balance modeling system. In: Mathematical Models of Small Watershed Hydrology and Applications,Vijay P. Singh, and Donald Frevert. (Editor).Water Resources Publication LLC., Highlands Ranch, CO, USA, pp. 555-590 Chapter 17), 2002

Zedler P.H., Life histories of vernal pool vascular plants, in: Ikeda D.H. and Schlising R.A., Vernal Pool Plants: Their Habitat and Biology. Studies from the Herbarium, No. 8, California State University. Chico, CA, 1990

Appendix:

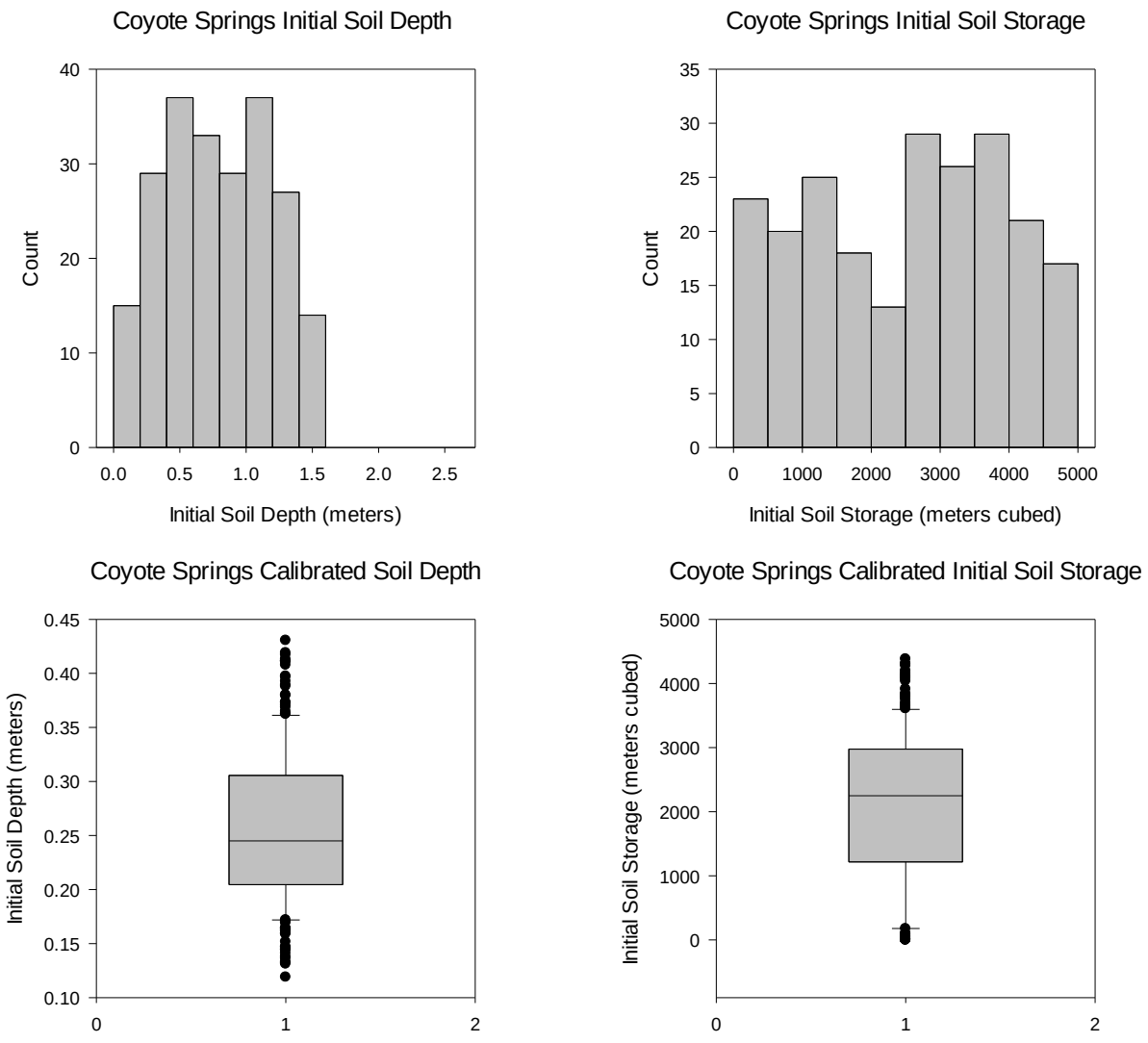

Figure 30. Histograms of initial values and boxplots of calibrated values from 200 Monte Carlo simulations for the parameters Soil Depth and Soil Storage for Coyote Springs

Initial values are the values that the model started calibration from and the calibrated values are the parameter values that the solver calibrated to.

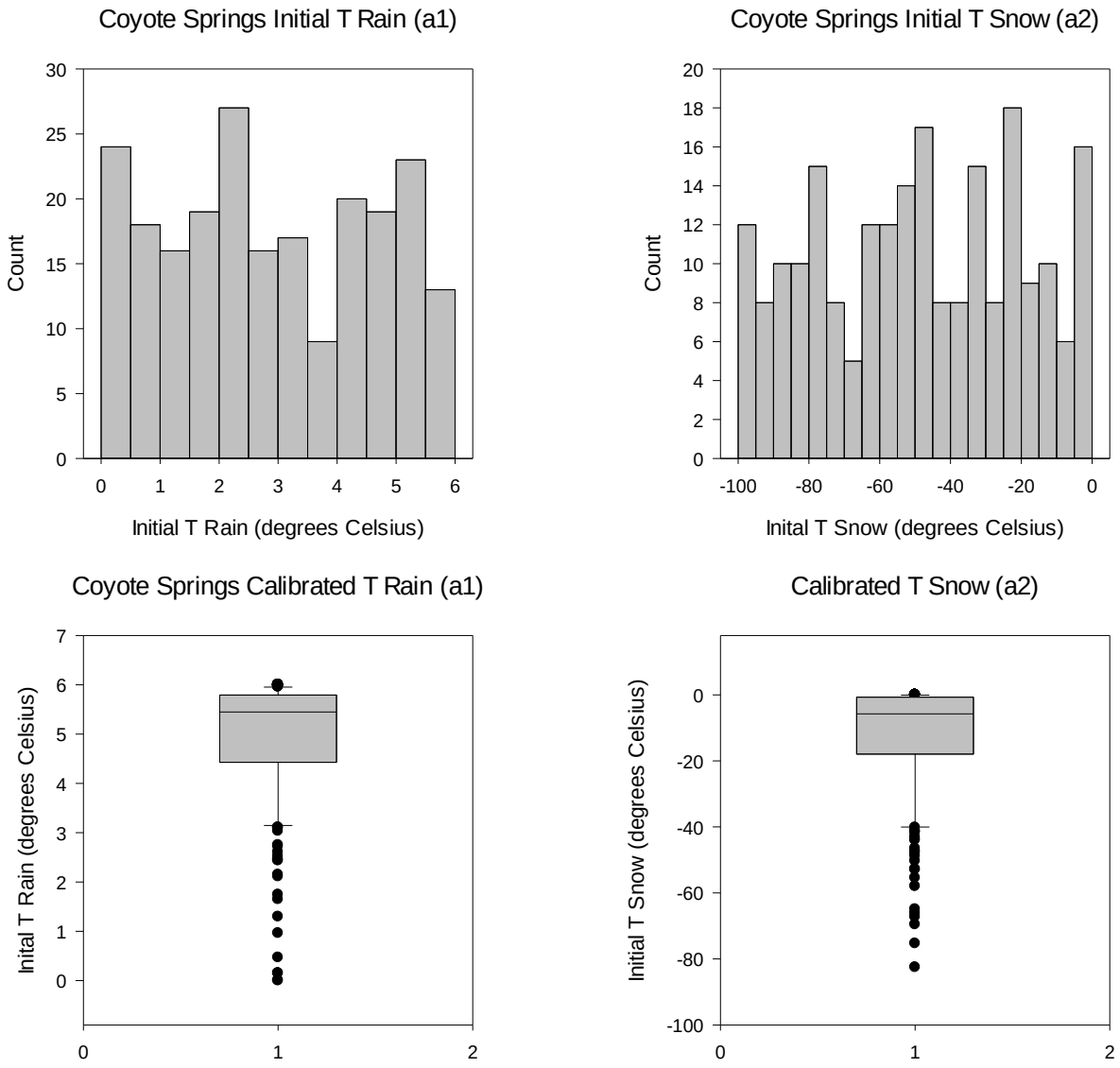

Figure 31. Histograms of initial values and boxplots of calibrated values from 200 Monte Carlo simulations for the parameters T Rain and T Snow for Coyote Springs

Initial values are the values that the model started calibration from and the calibrated values are the parameter values that the solver calibrated to.

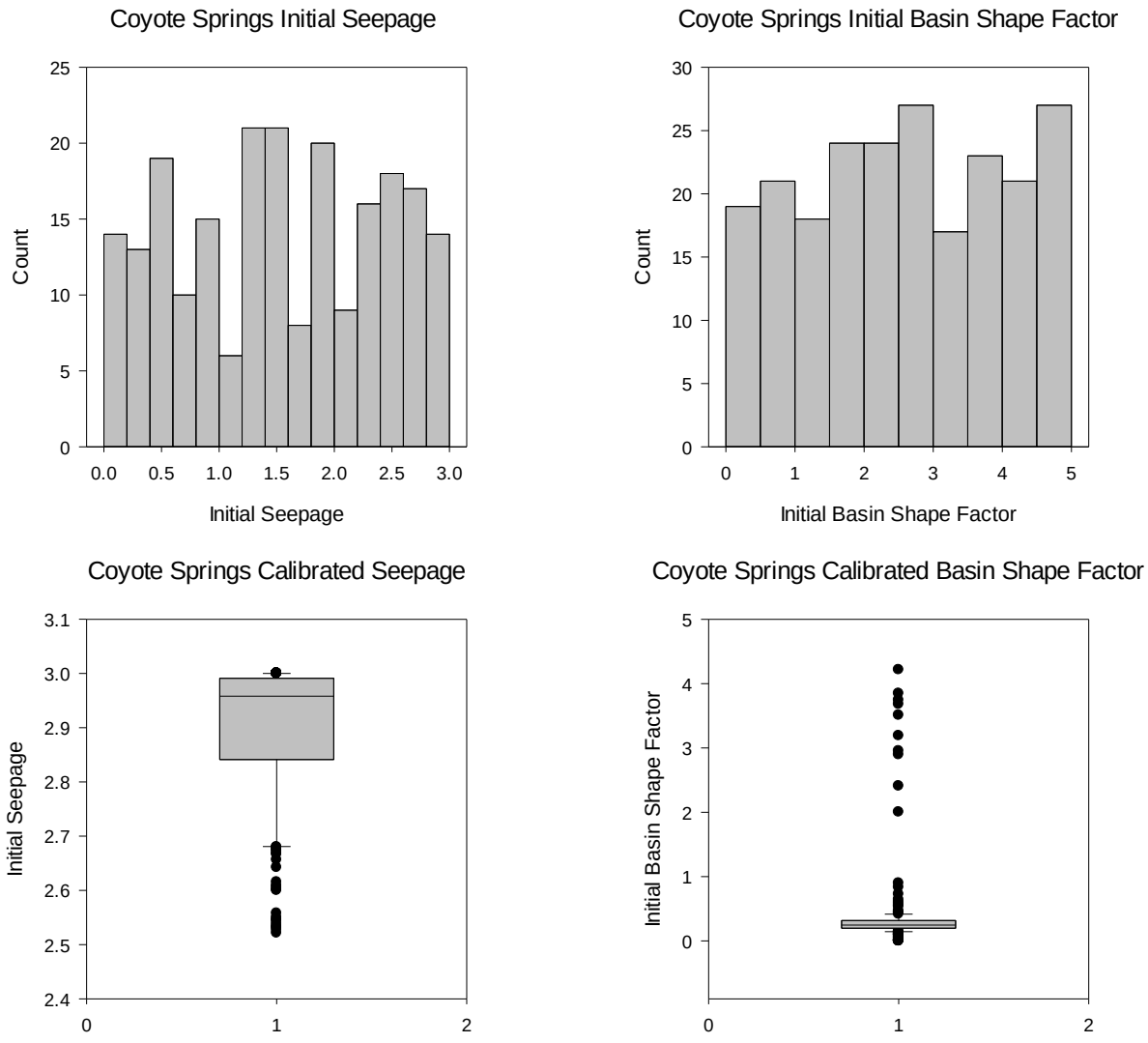

Figure 32. Histograms of initial values and boxplots of calibrated values from 200 Monte Carlo simulations for the parameters Seepage and Basin Shape Factor for Coyote Springs.

Initial values are the values that the model started calibration from and the calibrated values are the parameter values that the solver calibrated to.

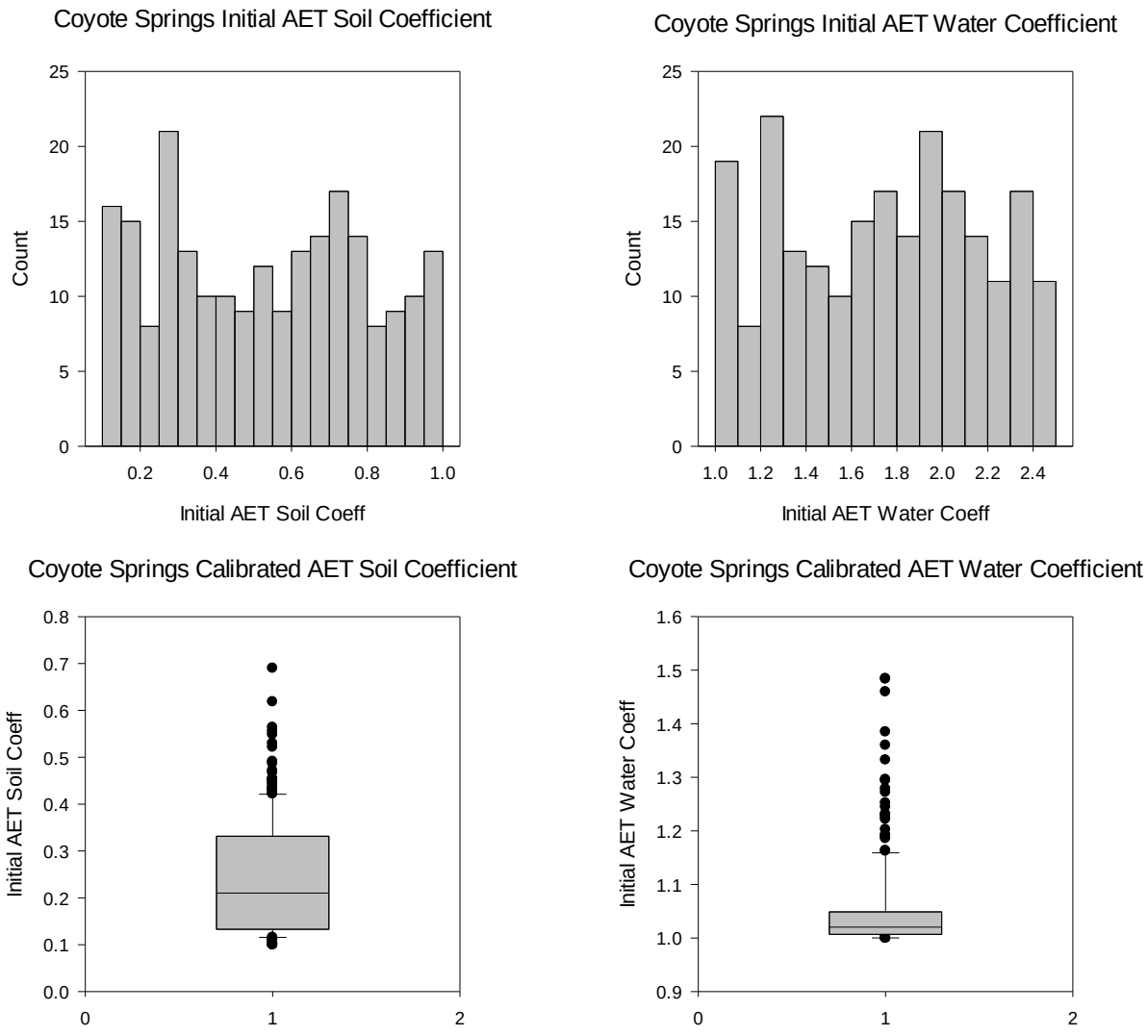

Figure 33. Histograms of initial values and boxplots of calibrated values from 200 Monte Carlo simulations for the parameters AET Soil and AET Water for Coyote Springs

Initial values are the values that the model started calibration from and the calibrated values are the parameter values that the solver calibrated to.